Optical Tweezers development as a tool for biomedical diagnosis

João Miguel de Freitas Oliveira
Master's in Medical Physics
Departamento de Física e Astronomia
2022

Supervisor
Prof. Dr. Pedro Jorge, Faculdade de Ciências da Universidade do Porto, INESC-TEC

Co-Supervisor
Prof. Dr. Nuno Silva, Faculdade de Ciências da Universidade do Porto, INESC-TEC

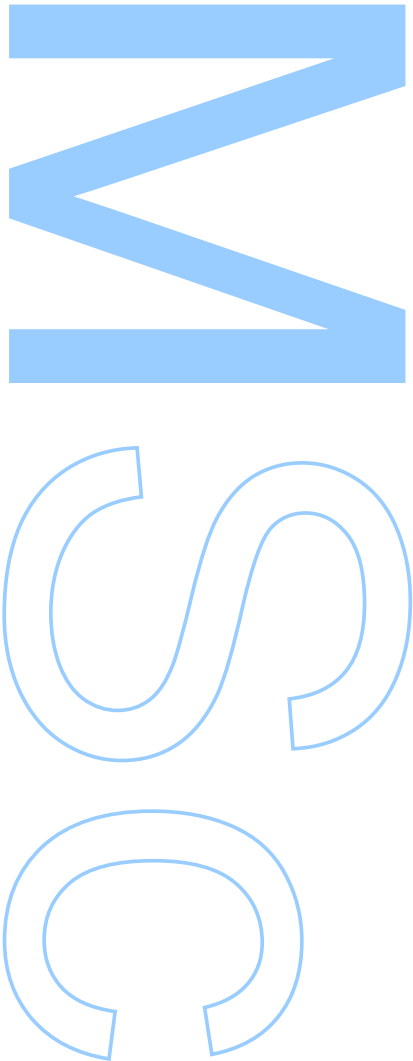

U.PORTO

FACULDADE DE CIÊNCIAS
UNIVERSIDADE DO PORTO

Todas as correções determinadas pelo júri, e só essas, foram efetuadas.

O Presidente do Júri,

Porto, _____/_____/_____

UNIVERSIDADE DO PORTO

MASTERS THESIS

Optical Tweezers development as a tool for biomedical diagnosis

Author:
João OLIVEIRA

Supervisor:
Prof. Dr. Pedro JORGE

Co-supervisor:
Prof. Dr. Nuno SILVA

A thesis submitted in fulfilment of the requirements
for the degree of MSc. Medical Physics

at the

Faculdade de Ciências da Universidade do Porto
Departamento de Física e Astronomia

December 14, 2022

"So Eden sank to grief, So dawn goes down to day. Nothing gold can stay. "

Robert Frost

Sworn Statement

I, João Miguel de Freitas Oliveira, enrolled in the master's degree in Medical Physics at the Faculty of Sciences of the University of Porto hereby declare, in accordance with the provisions of paragraph a) of Article 14 of the Code of Ethical Conduct of the University of Porto, that the content of this dissertation reflects perspectives, research work and my own interpretations at the time of its submission.

By submitting this dissertation, I also declare that it contains the results of my own research work and contributions that have not been previously submitted to this or any other institution.

I further declare that all references to other authors fully comply with the rules of attribution and are referenced in the text by citation and identified in the bibliographic references section. This dissertation does not include any content whose reproduction is protected by copyright laws.

I am aware that the practice of plagiarism and self-plagiarism constitute a form of academic offense.

João Oliveira

14/12/2022

Acknowledgements

The dissertation writing and working process is, in the end, a collaborative effort, something I have definitely felt over the past year. The challenges and obstacles that I faced required the assistance, personal or professional, of many people, and so I'd like to thank all who, in their own way, made this work a possibility.

First of all, I'd like to thank my supervisor, Dr. Pedro Jorge, for providing me the opportunity to take part in this project and allowing me to develop my skills in the field, all the while supporting my growth and potential. Thank you for the chance to integrate this team, and all the help you've given me.

I'd also like to thank my co-supervisor, Dr. Nuno Silva, for being ever present throughout my work and helping me overcome the many obstacles that appeared before me, whether it be day-to-day problems or more demanding issues. Thank you for your availability and dedication, it was truly appreciated.

To Dr. Teresa Borges, for providing me with the micro-algae samples, without which this dissertation would greatly suffer.

To my colleagues from the Center of Applied Photonics at INESC-TEC, Vicente Rocha, Duarte Silva and Tiago Ferreira, Felipe Coutinho and Joana Teixeira for not only helping me with the dissertation and the hardship it entails, but also for being a great group to work with or next to. A special thanks to Inês Carvalho, for all the assistance and support in the first steps and introduction to this dissertation, I'm very grateful. I'd also like to thank Porfírio Fernandes for the help given with some of the computational problems that arose.

On a more personal note, I'd like to thank João Pinho, Pedro Sousa, Leonardo Hügens, António Cesário, Tiago Lemos, Rui Peixoto, Tiago Gonçalves, David Lima, André Miranda, Brüno Costa, Ana Cacho and Vasco Ferreira, along with my friends from Sueca Italiana, for your friendship over these years, which would have been a lot less interesting without you.

To my parents, aunt, and siblings, Ricardo and Mariana, for the unconditional love and support you've given me. You've gifted me with more than I could ever repay, and for that I'm eternally grateful to you all.

To Inês Ornelas, for the love and kindness you have always offered me, especially in trying times, I'll be forever thankful in more ways than I can tell.

Lastly, but not least, I'd like to thank my family and closest friends for your unwavering belief and assistance.

UNIVERSIDADE DO PORTO

Abstract

Faculdade de Ciências da Universidade do Porto
Departamento de Física e Astronomia

MSc. Medical Physics

Optical Tweezers development as a tool for biomedical diagnosis

by João OLIVEIRA

Sensor development in biology and medicine has always been a primary focus in science, with contributions from various domains of thought coming together to solve an ever-present detection and diagnosis challenge. As it stands, the optical tweezers technique has witnessed a continuous increase in its use for these purposes, thanks to its capacity to trap and manipulate single cells in a non-invasive manner while obtaining reasonably fast results, showing to be a good tool for biotechnology use in general. Additionally, the smooth integration of modules and components into the system, seen in the plethora of alternative arrangements, advocates for the above, as does its relatively simple customization to meet the demands of users.

In this dissertation, we investigate the application of a conventional optical tweezers system as a potential biological sensor. We attempt to construct a classification technique with machine learning algorithms for real-time particle identification by collecting forward scattered light from the sample with the help of a quadrant photodetector. Three carefully selected case studies are employed to evaluate the classification tool's performance in different contexts, with a specific focus on the identification of bound and unbound states for Carboxy PMMA beads with a Streptavidin-Biotin complex functionalized on their surface, which is intended to mimic the behavior of molecular imprinted polymers. With the trapping of *Tetraselmis suecica* and *Tetraselmis sp.*, the separation between two different species of micro-algae is also attempted. We achieve an overall success rate of 75% for the categorization studies, indicating that the tool has the potential to be integrated into biomedical research and to be considered an option for the development of future sensors.

We also deploy a graphical user interface (GUI) for the usage of the optical tweezers setup as a result of this research, with the goal of smoothing out the data collecting procedure. The architecture of this interface, as it was constructed from the ground up, has the additional benefit of enabling novice users to collect data from the setup in a relatively simple manner, while allowing more advanced users to develop their own subroutines and methods to meet the requirements of their objectives.

UNIVERSIDADE DO PORTO

Resumo

Faculdade de Ciências da Universidade do Porto
Departamento de Física e Astronomia

Mestrado em Física Médica

Desenvolvimento de Pinças Óticas como ferramenta de diagnóstico biomédico

por João OLIVEIRA

O desenvolvimento de sensores na biologia e na medicina sempre foram uma tarefa de extrema importância no panorama geral da comunidade científica, com contribuições de ideias de todas as áreas do saber, culminando num único objetivo, a necessidade de deteção e diagnóstico nas áreas da saúde. Nos últimos tempos, a técnica das pinças óticas tem testemunhado uma aplicação crescente nestes campos da ciência devido à sua capacidade de aprisionar e manipular células individuais de uma forma não invasiva, e deste modo obter resultados relativamente rápidos, o que aponta para o seu potencial uso na tecnologia biomédica. Além disso, a integração simples de novos módulos e componentes no sistema, evidenciado pelas inúmeras configurações diferentes da montagem, demonstra novamente a sua utilidade, adicionando ainda a fácil modificação do sistema de modo a cumprir os objectivos particulares de estudo.

Nesta dissertação, a investigação da aplicação de um sistema convencional de pinças óticas como possível sensor biomédico é realizada. Para este fim, o desenvolvimento de um classificador automático utilizando métodos de *machine learning* é atentado, com o objetivo de conseguir a identificação de partículas em tempo real. Os dados são obtidos a partir da radiação de *forward scattering* da amostra aquando aprisionada, coletada a partir de um fotodetetor de quadrantes. São escolhidos três casos de estudo para avaliar a performance do classificador criado em diferentes contextos, focando-nos especialmente na identificação de estados ligados ou não de Carboxy PMMA beads cuja superfície foi funcionalizada com um complexo Streptavidin-Biotina, partícula esta escolhida para imitar o comportamento de *molecular imprinted polymers* (MIPs). Ainda assim, é tentada a categorização e distinção entre duas espécies de micro algas, sendo estas a *Tetraselmis*

suecica e *Tetraselmis sp.*. Obtivemos uma taxa de sucesso médio de 75%, resultado que aponta para o potencial uso deste protocolo na integração da nova geração de sensores biomédicos.

Como produto desta dissertação, apresentámos também uma interface gráfica (GUI) criada para agilizar o processo de recolha de dados. Este trabalho tem a finalidade de desenvolver uma ferramenta de uso fácil para utilizadores menos experientes, permitindo porém a utilizadores mais versados a possibilidade de desenvolver as suas próprias subrotinas, de modo a controlar o sistema da forma mais eficiente possível para o seu desígnio final.

Contents

List of Figures

Glossary

3D	Three Dimensions
OT	Optical Tweezers
PSD	Power Spectral Density
FOT	Fiber Optical Tweezers
HOT	Holographic Optical Tweezers
COT	Conventional Optical Tweezers
FFT	Fast Fourier Transform
EP	Equipartition
PCA	Principal Component Analysis
GUI	Graphical User Interface
ISO	International Organization for Standardization
DNA	Deoxyribonucleic Acid
DAQ	Data Acquisition Board
EVR	Explained Variance Ratio
PMMA	Polymethyl Methacrylate
PS	Polystyrene
QPD	Quadrant Photodetector
NA	Numerical Aperture
INESC-TEC	INESC Technology and Science
CMOS	Complementary Metal-Oxide-Semiconductor
KPZ	K-Cube Piezo Controller

KPA K-Cube Beam Position Aligner

LED Light Emitting Diode

TSG T-Cube Strain Gauge Reader

TEC Thermoelectric Cooler

MIP Molecular Imprinted Polymer

To my father Ricardo, my mother Agostinha and my aunt and godmother Rita, thank you for everything, I couldn't ask for a better family.

Chapter 1

Introduction

The need for better diagnosis and detection methods is a driving force for some of the advancements in science and of the highest importance to the field of medicine. Naturally, the development of new techniques in physics becomes a requirement of this pursuit, with the creation of reliable tools and sensors that provide better control and resolution to aid in all steps of treatment. It is unclear whether these implications were already considered by Arthur Ashkin when first describing the inner mechanisms of Optical Tweezers (OT) in 1970 [1], although the biological applications were later hypothesized when Ashkin and his team reported the trapping of several dielectric particles [2] and single cells [3, 4]. Yet, it is now indisputable that OT constitutes a valuable manipulation and control tool for some of the most advanced applications in biology and medicine [5, 6].

Since the development of single-optical beam trapping in 1986, OT became a common piece of equipment in many academic research laboratories that work on imaging and biophotonics. From simpler and commercial designs to more specific and versatile ones, there are multiple implementations with a wide range of features depending on the application. Nevertheless, while the optical design and assembly are often sufficient to deploy high-performance equipment that can be used to manipulate mesoscopic particles, turning it into a useful tool that can be operated at different levels of expertise often require in-house development of automation software that is often overlooked by the optical suppliers. Furthermore, having such control on the operation framework is highly desirable for integrating new models and methodologies that are constantly emerging from fundamental research.

Within this context, the present document reports our efforts to deploy a modular control framework and integrated software solution, capable of turning our OT experimental

setup into an automatic OT system. In addition, by merging it with machine learning classification methodologies and automatic trapping algorithms that were previously explored by our research group, we demonstrate how these tools can be easily integrated into the computational toolbox developed, thus paving the way for the development of autonomous biomedical diagnostic tools.

1.1 A brief history of Optical tweezers

The inner workings of OT involve a fine balance between optical forces. The first recorded observation of optical forces was made by Kepler in 1619, who postulated the presence of radiation pressure by observing the comet tails pointing away from the Sun. Later, Maxwell provided a mathematical framework for the momentum of the electromagnetic wave, but it was only in 1970 that Ashkin observed for the first time the trapping of transparent dielectric spheres. At the time, the configuration used involved a balance of the scattering force of two counter-propagating fields, which strongly limited the manipulation in three dimensions [1]. In spite of obvious limitations, this idea seed the work of optical molasses, using multiple laser beams to cool and trap atoms, which eventually awarded Chu, one of Ashkin's former colleague, the Nobel Prize in 1997. In its turn, Ashkin itself was awarded the Nobel Prize only 21 years later, in 2018, but for the discovery of a distinct configuration of OT that paved for three-dimensional trapping and manipulation of particles.

Indeed, in 1985, Ashkin and his colleagues demonstrated that using a high numerical aperture (NA) objectives, they were able to tightly focus the beam to a point where spatial intensity variations close to the focal spot could create a mensurable gradient optically-induced force. With this new component, a balance between the radiation and gradient optical forces was achieved and the effective 3-dimensional trap was finally deployed, eventually becoming known as the Optical Tweezers. Indeed, and to this day, this single-beam trap is the most common configuration for the conventional laboratory setups of OT. Most of the time, it makes use of an invert microscope configuration, using the same objective to focus and image the system. Since its first realization, the applications of this system quickly sprout in many distinct research fields and now span from simple manipulation procedures, such as controlling and moving single particles [3, 7], to the most complex tasks, such as unfolding DNA [8, 9].

The advent of the optical trapping phenomenon brought forth research in its use in a wide array of fields, such as biology and medicine. As such, several approaches were attempted toward this end, with increasingly better sensors and measurements. Naturally, adjustments in the usual setup, named conventional optical tweezers (COT), were necessary to meet the needs and aims of each experiment, leading to a vast array of distinct configurations with specialized functions and strengths.

One way to increase the versatility of the COT system is to add arbitrary potential shaping capabilities, which is called the holographic optical tweezers setup (HOT), displayed in Figure 1.1a. This approach uses computer-generated holograms to construct 3D configurations of single beam traps [10, 11], imprinting them onto the beam wavefronts with a diffractive optical element such as a Spatial Light Modulator. This beam is then focused onto the sample plane by a high numerical aperture objective lens, creating an arbitrary shaped trap that can also be controlled in time [10]. This configuration is one of the most versatile setups for optical trapping but presents some caveats for quantitative analysis. Indeed, simple tasks such as stiffness calculations are often too cumbersome [12], since exact knowledge of the interaction between the focused beam and the target particles is required. Furthermore, the same bulkiness problems present in COT arise with this configuration, making its use in miniaturized biomedical sensors harder to implement.

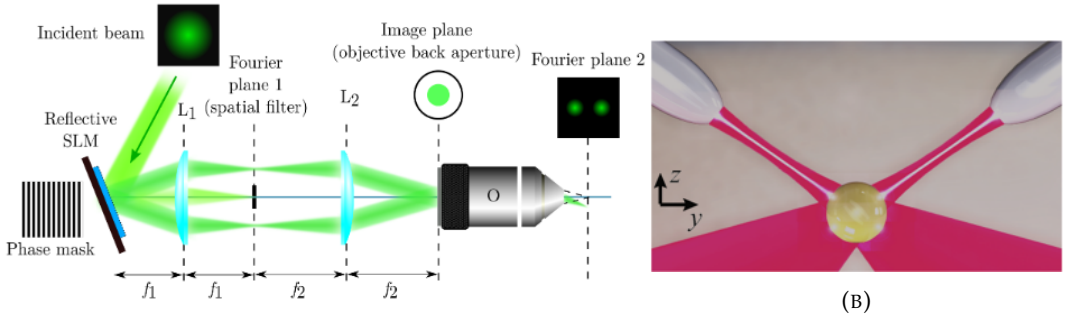

(A) (B)

FIGURE 1.1: (A) A holographic optical tweezers setup, with a spatial light modulator [12] (B) A dual fiber optical tweezers setup [13].

Fiber optical tweezers are another alternative setup that features as main advantages their versatile manipulation, compact design and straightforward production [14]. Although the initial descriptions of the procedure required two optical fibers for the trapping [15], as seen in Figure 1.1b, later uses of the technique describe the attainment of optical trapping using only a single optical fiber [16]. The mechanisms of FOT are somewhat similar to conventional trapping, although differing on key elements. The end of

the fiber is modified to have a lens shape, in order to achieve the focusing of the light, improving the trapping stability from the normal setup [17]. Thus, comparing with the COT setup, it does not require beam steering components nor high numerical aperture objectives for focusing. This reduces the bulkiness of COT and provides a much easier fabrication process, all the while obtaining a strong gradient force from the trapping laser. Additionally, this approach also has the advantage of working on turbid media and having a better trapping efficiency [18] than the usual objective focusing, with the drawback of a less tightly focused beam reducing the efficiency of the trap for larger particles or three-dimensional manipulation. Nonetheless, this technology is a strong contender for the construction of compact optofluidic devices, extending the optical trapping towards a biological tool [19].

Finally, and more recently, the advent of plasmonics in the beginning of the XX century opened the door to the trapping of particles at nanometric scales, which is typically hard to obtain in the COT due to the diffraction limit. This possibility stems from the ability of generating highly localized evanescent fields, confining light in scales below the optical wavelength that can be used to trap particles with the strong gradient forces at low electromagnetic powers [6]. From metal tips [20] to plasmonic films [21] and fiber tips [22], multiple configurations has been explored in the literature with varying degrees of success, and are now one of the most active fields of research in the fundamental aspects of OT.

1.2 Applications of OT and Motivation

Applications of OT can be divided in two broad families: the use of OT for manipulation, precisely controlling the position of the trapped particle and immobilizing it for distinct purposes, and the use of OT for probing properties of the trapped specimen by using information gathered from the scattered optical signal or directly from the image.

Concerning the use for manipulation purposes, the optical tweezers technique has been used in a broad spectra of contexts, as its capabilities of inducing forces and spatial trapping come across as particularly useful in the study of molecular dynamics with force spectroscopy [23], since the method is especially sensitive to low intensity forces, and pipette making [24]. Another interesting application is the immobilization of the particle, which can be crucial to assist in techniques that require large acquisition times and in particular when the target is freely moving in a liquid. One of the most remarkable

applications in this field is the Raman tweezers, where a second laser is used to excite Raman scattering in the trapped particle, collecting the signal with a spectrometer and analysing the spectrum searching for characteristic molecular signatures [25].

In what reports to the probing properties of the trapped specimen, applications in the field of microrheology have been numerous and diverse in the framework of the optical tweezers [26]. In order to determine strain and stress properties of soft materials, the mechanical response of these materials must be studied through precise application of low intensity forces. Furthermore, the ability to apply a localized strain in a section of a material and the direct measurement of shear response allow for a better description of its properties, instead of bulk rheology methods, that rely on averaged quantities measured from the macroscopic sample [27]. The optical trapping effect has been proven to be valuable in the study of brownian motion utilizing drift analysis [28]. Because particles interact hydrodynamically with one other in a colloidal solution, their diffusion coefficient and drift velocity can be estimated by measuring inter-particle distance, validating statistical physics' theoretical predictions. Because these properties vary in parallel and perpendicular directions relative to the particle's motion, reliable tracking of relative positions is critical. This necessitates the employment of optical systems, as the proportions of the problem demand a setup with high resolution at these scales. It is worth mentioning the use of OT in inducing colloidal phase transitions and probing other important phenomena such as critical Casimir forces [29]. These relatively recent trends have investigated the approach in the experimentation of numerous non-equilibrium predictions, e.g. optical lattice phase transitions [30, 31].

Focusing on biology and medicine, the use of the optical tweezers technique opened multiple opportunities for its potential use in a more diagnostic and treatment oriented scenery. There were numerous approaches for this demanding undertaking in the past, mostly hinging on DNA manipulation [32–34], cell sorting [35, 36] and cell motility [37, 38]. Progress in these areas has also paved the way for an optical trapping lab-on-a-chip methodology, further pushing the technique as a suitable choice for this enterprise.

More recently, researchers at the Center for Applied Photonics (CAP) at INESC-TEC, in conjunction with iLoF, exploited the possibility for a cell classification tool in a diagnosis setting. Paiva et al. reported the classification of human cancer cells using optical tweezers and machine learning algorithms for the identification, arguing that the changes

in fundamental cellular processes can alter the particles behavior under trapping conditions relative to their healthy counterparts, allowing categorization to be achievable. Additionally, observed time intervals of 2.3 seconds and 90% accuracy highlight the method's potential for biomedical applications.

Continuing this line of research, Carvalho et al. reported the particle classification using forward scattering light in an optical tweezers setting. This study stated a ≈90% success rate in the identification of non-organic particles with signal segments of 500 milliseconds also using machine learning methods for the task at hand. The comparison of these two approaches can be found in Jorge et al. [40], where the different setups were benchmarked with the same materials: non-organic materials and nanometric sized particles.

Alongside this development, researchers at the University of Campania Luigi Vanvitelli have explored the use of plasmonic optical fibers for the detection of molecular imprinted polymers (MIPs) [41, 42]. This advancement is of great interest for the biomedical sensor field, since the consistency of these molecules in sensing target proteins has been demonstrated in various studies [42], possibly contributing to a new generation of sensors. Thus, we may anticipate that these MIPs can also be used to discriminate for the presence of nanosized biomarkers using the forward scattered signal in OT setups, but their detection with OT is still unexplored, as production issues arise when creating the necessary cavities in the polymer matrix [43].

In spite of all this potential, one still finds challenges when adapting standard commercial versions of OT setups as these are typically not suitable for establishing a versatile diagnostic device. In particular, these lack software versatility and integrated frameworks to cope with the high-throughput and high-level usability required for such purpose. In this way, it requires the development of a useful computational toolbox, capable of delivering easy and reproducible results of the scattering signal of many particles in each sample in optimized and automatic manners. For this purpose, we need to design and develop new control and software solutions to adapt our commercial version COT, which will be the key motivation of this dissertation.

1.2.1 Objectives and outline of the dissertation

The operational objectives of this work are straightforward, as these stem from the natural progression of the motivations that led to their necessity. Given the current conditions of

the problems we wish to address, the operational objectives are:

- Explore the concept of an optical tweezers setup, performing calibrations and measurements that are as accurate as possible;
- Develop drivers to automate and control our in-house OT setup in a modular and integrated manner;
- Develop a Graphical User Interface (GUI) to ease the data acquisition process and shape the capabilities of the setup to suit our specific needs;
- Deploy a real-time classification tool for the identification of trapped particles, based on previously developed algorithms;
- Present a proof-of-concept of the system with a special focus on biomedical and biology applications focusing on three case studies: i) classification of synthetic particles, for testing the algorithm; ii) identification of molecular imprinted polymers (MIPs), furthering both the techniques and the use of MIPs as possible diagnostic tools; and iii) the classification of two different species of micro-algae, showing the potential for the categorization for other living cells.

Describing the methodology and reporting our efforts to achieve these goals, this dissertation organizes as follows:

Chapter 1: A small introduction, complete with a historical context of optical tweezers, state-of-the-art overview, and motivation for the dissertation. Objectives for this document are also outlined;

Chapter 2: A physical description of the optical trapping phenomena in different optical limits and Brownian motion. Additionally, a synopsis of the analysis methods used throughout the document and a brief explanation of the experimental setup and its components;

Chapter 3: A characterization of the performed calibrations and developed data analysis protocols;

Chapter 4: An overview of the graphical user interface designed to aid in experimental flow and system control;

Chapter 5: Utilization of classification tools in three distinct case studies: synthetic particles, molecular imprinted polymers and micro algae, along with a discussion of the obtained results;

Chapter 6: A summary of the findings acquired with this work, as well as a proposal of future work to be completed;

1.3 Original Contributions

In addition to the present document and in close collaboration with the other elements of the OT team at the Center for Applied Photonics at INESC TEC, this MSc dissertation resulted in several communications and outputs namely:

Conference Peer-Reviewed Proceedings:

- J. Oliveira, V. Rocha, A. Guerreiro, P. A. S Jorge, and N. A. Silva, "Automation strategies and machine learning algorithms towards real-time identification of optically trapped particles", EOSAM Conference Proceedings, 2022
- V. Rocha, J. Oliveira, A. Guerreiro, P. A. S Jorge, and N. A. Silva, "Intelligent Optical Tweezers with deep neural network classifiers", EOSAM Conference Proceedings, 2022, to appear
- J. Teixeira, V. Rocha, J. Oliveira, P. A. S. Jorge, and N. A. Silva, "Towards real-time identification of trapped particles with UMAP-based classifiers", AOP Conference Proceedings, 2022
- F. Coutinho, J. Teixeira, V. Rocha, J. Oliveira, P. A. S. Jorge, and N. A. Silva, "Autonomous Optical Tweezers: from automatic trapping to single particle analysis", AOP Conference Proceedings, 2022

Oral Presentations

- J. Oliveira, **V. Rocha**, N. A. Silva, P. A. S. Jorge, "Optical Tweezers development as a tool for biomedical diagnosis", Investigação Jovem da U. Porto, 2022.
- J. Oliveira, **V. Rocha**, N. A. Silva, P. A. S. Jorge, "Optical Tweezers development as a tool for biomedical diagnosis", Física 2022.

- J. Oliveira, **V. Rocha**, N. A. Silva, P. A. S. Jorge, "Automation strategies and machine learning algorithms towards real-time identification of optically trapped particles", EOSAM, 2022.

Poster Presentations:

- V. Rocha, J. Oliveira, A. Guerreiro, P. A. S Jorge, and N. A. Silva, "Deep-learning approach to classification of optically trapped particles", Investigação Jovem da U. Porto, 2022.
- V. Rocha, J. Oliveira, A. Guerreiro, P. A. S Jorge, and N. A. Silva, "Recurrent Neural Network classification of optically trapped particles", Física, 2022.
- V. Rocha, J. Oliveira, A. Guerreiro, P. A. S Jorge, and N. A. Silva, "Convolution Neural Network classification of optically trapped particles", EOSAM, 2022.
- J. Teixeira, V. Rocha, J. Oliveira, P. A. S. Jorge, and N. A. Silva, "Towards real-time identification of trapped particles with UMAP-based classifiers", AOP, 2022
- F. Coutinho, J. Teixeira, V. Rocha, J. Oliveira, P. A. S. Jorge, and N. A. Silva, "Autonomous Optical Tweezers: from automatic trapping to single particle analysis", AOP, 2022

Chapter 2

Optical tweezers: from theory to the experimental Setup

This second chapter divides into two structural sections, first covering the theoretical concepts of OT before advancing to the description of the experimental setup.

In the first section, we briefly introduce the underlying physical principles of OT systems, understanding the trapping mechanisms and optically-induced forces that come into play in distinct regimes based on particle size. Then, accounting for the stochastic and viscosity effects of the immersion, we provide an effective model for the trapped particle based on the Langevin equation. Lastly, by focusing on the case of the single-beam gaussian trap, we show how it is possible to extract the governing physical parameters from experimental observations, in order to calibrate our model and extract meaningful particle properties.

In the second section, we describe in detail the experimental setup used throughout this dissertation, as well as the tools used to retrieve the necessary data for calibration and further classification procedures.

2.1 Physical principles of Optical Tweezers

The optical trapping phenomenon involves an equilibrium of forces caused by emitted photons from a radiation source acting on a dielectric particle. These forces are consequences of the conservation of electromagnetic momentum and are understood to hail from two distinct effects: the scattering of the incoming photons and the intensity gradient of the beam shape. Both of these components arise naturally from the theoretical

treatment of the optical forces that the particle endures, which depends on the relationship between the wavelength and the particle size. This comparison can be made using a *size parameter* [44] to establish the range of validity of the approximations,

$$\xi = 2\pi a n_{\mathrm{m}} / \lambda_0 \tag{2.1}$$

where a is the radius of the particle, n_m is the refractive index of the surrounding medium, and λ_0 is the laser vacuum wavelength. This measure relates the characteristic diameter of the particle to the scale of the photon wavelength in the surrounding medium, with $\xi \ll 1$ ($a \ll \lambda_0$) being called the dipole approximation regime and $\xi \gg 1$ ($a \gg \lambda_0$) being the ray optics regime.

2.1.1 Dipole Approximation regime

The dipole approximation regime is the easiest to analyze in an analytical and mathematical manner, and thus important to understand the two optical forces that come into play in OT. Within this regime, the $a \ll \lambda_0$ approximation becomes valid, which means that the particle size is much smaller than the wavelength. In light of this aspect, we can consider the particle to be described as a point dipole as

$$\mathbf{p}_{\mathrm{i}} = \alpha_i \mathbf{E}_{\mathrm{i}} \tag{2.2}$$

where $\mathbf{p}$ is the electric dipole moment vector, α_i is the polarizability of the particle and $\mathbf{E}_{\mathrm{i}}$ is the incident field. The interaction of the dipole with the electromagnetic field is well described in the Maxwell framework, which assuming a negligible curl-spin component, results into [45]

$$\mathbf{F}_{\mathrm{DA}} = \frac{n_{\mathrm{m}} \sigma_{\mathrm{ext}}}{c} \mathbf{S}_{\mathrm{i}} + \frac{1}{4} \alpha'_{\mathrm{p}} \nabla \left| E_{\mathrm{i}} \right|^2 \tag{2.3}$$

with α_{p} being the real part of the complex polarizability, n_{m} the medium refractive index, σ_{ext} is the particle extinction cross-section and $\mathbf{S}_{\mathrm{i}}$ is the time-averaged Poynting vector of the incident electromagnetic field.

The first component in right-hand side of equation 2.3 corresponds to the scattering term of the applied force that arises from absorption of light by the dipole [46], which is evident by the fact that it is proportional to the particle extinction cross-section. This component points in the propagation direction, i.e. the same direction of the Poynting vector $\mathbf{S}_{\mathrm{i}}$, as described in eq. 2.3, which means that it is not possible to trap a particle using only the scattering force of a single optical beam.

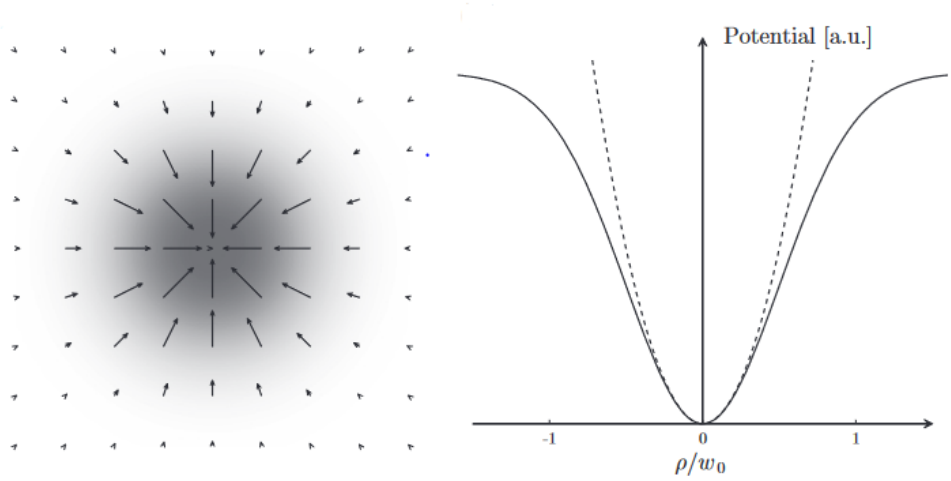

FIGURE 2.1: Gradient map (left) and potential well (right) due to gradient force [45].

To counterbalance that, there is a second term of eq. 2.3 whose contribution is proportional to the gradient of the electric field, and thus can be used to confine the particle. In particular, if the beam has a gaussian shape, the intensity profile takes the form

$$I_{\mathrm{i}}(\rho) = I_0 \mathrm{e}^{-\frac{2\rho^2}{w_0^2}} \tag{2.4}$$

where ρ is the radial component of the transverse plane, w_0 is the beam waist and I_0 is the maximum intensity, represented on figure 2.1 (left). Admitting a small displacement from the beam axis ($\rho/w_0 \ll 1$), the intensity profile can be approximated using the first terms of its Taylor series:

$$I_{\mathrm{i}}(\rho) \approx I_0 \left(1 - 2\rho^2/w_0^2\right) \tag{2.5}$$

The beam intensity profile has a direct effect on the force that the trapped particle endures. Using the well known relation $I_{\mathrm{i}} = \frac{1}{2} c n_{\mathrm{m}} |E_{\mathrm{i}}|^2$ for electromagnetic waves, we arrive at an expression for the force in terms of the intensity in eq. 2.6. It becomes clear that within the small displacement approximation, the applied force assumes a restorative quality in the radial component, producing a 3-dimensional optical trap. In fact, this phenomenon can be interpreted as a spring-like interaction, as in eq. 2.7, with a spring constant containing information pertaining to the incident beam and the surrounding medium.

$$\mathbf{F}_{\mathrm{grad}}(\mathbf{r}) = \frac{1}{2} \frac{\alpha'_{\mathrm{p}}}{c n_{\mathrm{m}}} \nabla I_{\mathrm{i}}(\mathbf{r}), \tag{2.6}$$

$$F_{\mathrm{grad},\rho}(\rho) = -\kappa\rho \text{ with } \kappa = 2\frac{\alpha'_{\mathrm{p}}}{c n_{\mathrm{m}}} \frac{I_0}{w_0^2}. \tag{2.7}$$

Knowing the form of the forces acting on the system, it can be assumed that the optical potential is of a quadratic shape, which can be seen in Figure 2.1 (right), while presupposing the small displacement approximation. This information is useful in the determination of the position distribution, as later described in this section.

2.1.2 Ray Optics regime

When the particle is much larger than the wavelength, the dipole approximation breaks down and the interpretation of the trapping phenomena become more complex, involving ray optics arguments and calculations. Nevertheless, it is still possible and feasible to describe it in qualitative terms, without entering in cumbersome calculations.

To accomplish this, we start by considering a particle with a refractive index of n_a in a non-magnetic surrounding medium of refractive index $n_m < n_a$ and irradiated by a laser beam with a wavelength in vacuum of λ_0. The incoming field, which can be thought of as a group of rays propagating in a straight line in this regime [47], will interact with the particle, being reflected and transmitted on the surface. This process results in an effective force equal and opposite to the change in momentum that each photon or ray undergoes.

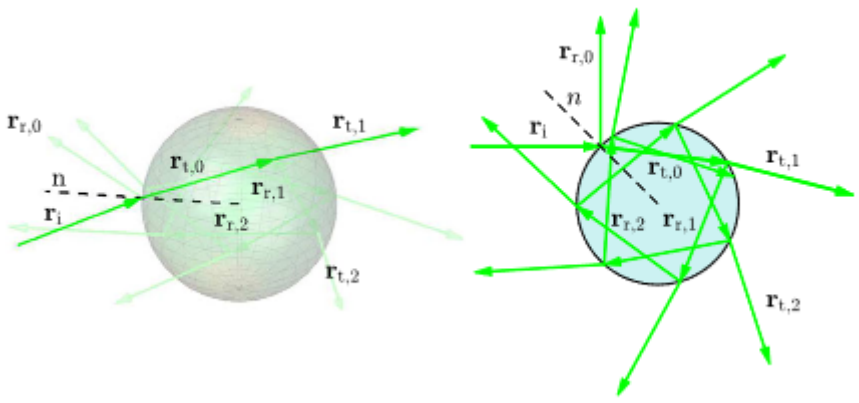

FIGURE 2.2: Incident ray undergoes reflection and refraction inside the particle, 3D and 2D view [44].

A schematic of the ray geometry can be seen on Figure 2.2. Each ray that passes through the particle transfers some of its momentum after an interaction proportionally to the fraction of the beam power P_i it carries, such that $P_{total} = \sum_i P_i$. Upon incidence on the particle surface, a fraction of the ray gets reflected, while the remaining is transmitted into the particle medium. This transmitted ray will endure the same interaction once it reaches the next boundary and so on until all the energy has been spent, meaning that,

by conservation of momentum [48], the force experienced by the particle in its center of mass is equal to,

$$\mathbf{F}_{\text{ray}} = \frac{n_{\text{m}} P_{\text{i}}}{c}\hat{\mathbf{r}}_{\text{i}} - \frac{n_{\text{m}} P_{\text{r}}}{c}\hat{\mathbf{r}}_{\text{r},0} - \sum_{j=1}^{+\infty} \frac{n_{\text{m}} P_{\text{t},j}}{c}\hat{\mathbf{r}}_{\text{t},j} \tag{2.8}$$

where $\hat{\mathbf{r}}_{\text{i}}$ is the unitary vector in the direction of the incident ray, $\hat{\mathbf{r}}_{\text{r},0}$ in the direction of the first reflected ray and $\hat{\mathbf{r}}_{\text{t},j}$ in the direction of j-th transmitted ray.

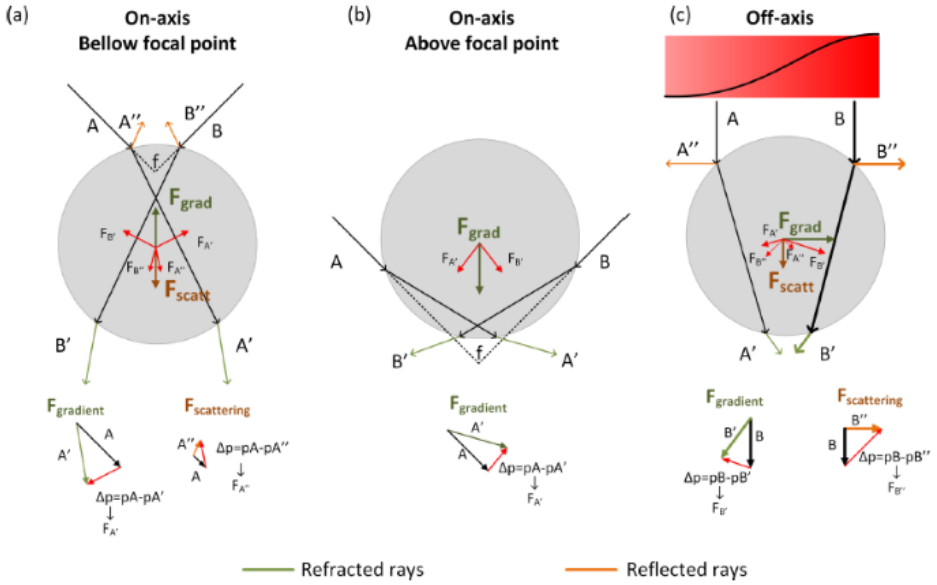

FIGURE 2.3: Scattering and gradient forces acting on a spherical particles [49].

Thus, the propagating directions and the forces they impinge on the particle divide nicely into two components, as it happens for the dipole regime: one that is always in the direction of the incident ray, and that can be considered the scattering force (F_{s}); and a second one that depends on the position of the particle, which we can call the gradient force (F_{g}), as displayed in Figure 2.3. Furthermore, for a tightly focused beam, one can see that there is a small component of the gradient force along the propagation axis that points towards the focus. This means that for specific conditions, a balance between scattering and gradient forces can occur in a position of equilibrium (slightly below the focal spot) where the particle will thus be trapped [50]. This regime is the setting for most of our work, given the chosen particles and wavelength scales. However, this ray optics formulation requires simulations to obtain the necessary features we expect to extract from the gathered data, forcing us to procure a more effective model for optical trapping analysis.

2.1.3 An effective model for the optically trapped particle

Although optical forces play a major role in particle dynamics, the fact that the particle is immersed in a medium at a given temperature means that other dynamics come into play. In particular, two important factors are the viscosity of the medium that dissipates the kinetic energy, and the particle collisions with the molecules of the medium in a random fashion. In other words, this means that the particle will undergo a Brownian-like motion. Therefore, we can deploy an effective model for the center of mass of the optically trapped particle by making use of the Langevin equation [12, 51] for a particle with mass m in a viscous fluid, namely

$$m\frac{\mathrm{d}^2}{\mathrm{d}t^2}r(t) = -\gamma\frac{\mathrm{d}}{\mathrm{d}t}r(t) + \chi(t) \tag{2.9}$$

where γ is the friction coefficient given by $\gamma = 6\pi\eta a$, for a sphere of radius a and drag coefficient η (Stoke's Law), and $\chi(t)$ is a random force with a mean value of 0 that is independent of the position of the particle, normalized to $\chi(t) = \sqrt{2S}W(t)$, where S is the intensity of the noise and $W(t)$ is known as the *white noise function*. Adding the optical induced force, eq. 2.9 takes the form of:

$$m\frac{\mathrm{d}^2}{\mathrm{d}t^2}r(t) = -\gamma\frac{\mathrm{d}}{\mathrm{d}t}r(t) + \chi(t) + F(r) \tag{2.10}$$

where $F(r)$ is responsible for confining the particle to the trap center. For the case of a single beam with a gaussian shape and considering small displacements, we can fit the model to the trapping conditions by approximating the force using the Hooke law $F(r) = -\boldsymbol{\kappa} \odot \boldsymbol{r}$ as previously discussed, being $\boldsymbol{k}$ a parameter that describes the trap and usually called its stiffness, and $\odot$ the Hadamard product. Furthermore, under the low Reynolds number approximation, the second derivative term can be dropped, resulting in a simplified overdamped Langevin model,

$$\frac{\mathrm{d}}{\mathrm{d}t}r(t) + \frac{\boldsymbol{\kappa}}{\gamma} \odot \boldsymbol{r} = +\xi(t) \tag{2.11}$$

where $\xi(t) = \sqrt{2D}W(t)$ and D is known as the diffusion coefficient, given by the Einstein-Smoluchowski relation $D = \frac{\kappa_B T}{\gamma}$.

2.1.4 Calibration procedures

Having set the simplified model, which is valid for small microscopic particles and sufficiently large times (milliseconds and above), we now explore how we can match the

theoretical predictions and observations defining some calibration procedures.

From the many methods that are well described in the literature [12, 44], we will focus on the equipartition and power spectral density methods, which were chosen for their simplicity or robustness. Besides calibration purpose, these methods will also play a role in training machine learning algorithms in order to classify particles as we will later see in Chapter 5.

2.1.4.1 Equipartition Theorem Method

The first method uses one of the tenements of statistical physics, the equipartition theorem. If the scattering force is of sufficiently small contribution, the system can be considered conservative [52], meaning we can assume a harmonic potential in each of the directions, e.g.

$$\mathrm{U(x)} = \frac{\kappa_x}{2}(x - x_{eq})^2 \tag{2.12}$$

where x_{eq} is the equilibrium position of the trap. Then, by the equipartition theorem, the time averaged value of this potential energy for each degree of freedom is given by $\frac{\kappa_B T}{2}$ (the time averaged value replaces the ensemble average due to the ergodic condition [53]), meaning that we have

$$\big\langle \mathrm{U(x)} \big\rangle = \big\langle \frac{\kappa_x}{2}(x - x_{eq})^2 \big\rangle = \frac{\kappa_B T}{2} \tag{2.13}$$

From this expression, we can easily extract the stiffness coefficient by taking the time averaged variance of the position of the trapped particle in the chosen direction, leaving us with

$$\kappa_x = \frac{\kappa_B T}{\big\langle (x - x_{eq})^2 \big\rangle}. \tag{2.14}$$

The value of this approach lies in its computational simplicity and speed, although it is more susceptible to noise and systematic errors.

2.1.4.2 Power Spectral Density Method (PSD)

A distinct methodology is to take the first order differential equation, and to solve it in the Fourier space. After neglecting leakage terms [51], we obtain the power spectrum formula in the shape of a lorentzian function

$$\mathrm{P(f)} = \big\langle |\tilde{r}(f)|^2 \big\rangle = \frac{1}{2\pi} \frac{D}{f_c^2 + f^2} \tag{2.15}$$

with f_c being the corner frequency, of value $f_c = \frac{\kappa_r}{2\pi\gamma}$. By obtaining the value of this frequency and γ through sampling the position of the particle and fitting the power spectral density to the lorentzian function, we are able to determine the value of the spring constant for both transversal directions x and y. The use of the PSD method is a standard tool in OT analysis since it is useful to detect electric and ambient noise, which appear as peaks in the frequency spectrum, while also minimizing the repercussions of mechanical drift at low frequencies [12, 51].

2.2 Overview of the Experimental Setup

For the purpose of this work, the experimental setup used is modular OT setup, the OTKB Modular Optical Tweezers System by Thorlabs, depicted in Figure 2.4. A schematic of the setup can be found in Figure 2.5. This setup is essentially constructed upon a standard inverted microscope optical tweezers design mounted on an actively isolated optical table, completed with a sample stage with nanopositioning capabilities through the piezo actuators, a quadrant photodetector for position detection, and a CMOS camera for image and video capture. Its modular configuration is of great advantage, easing the assembly stage and allowing the incorporation of new components as needed.

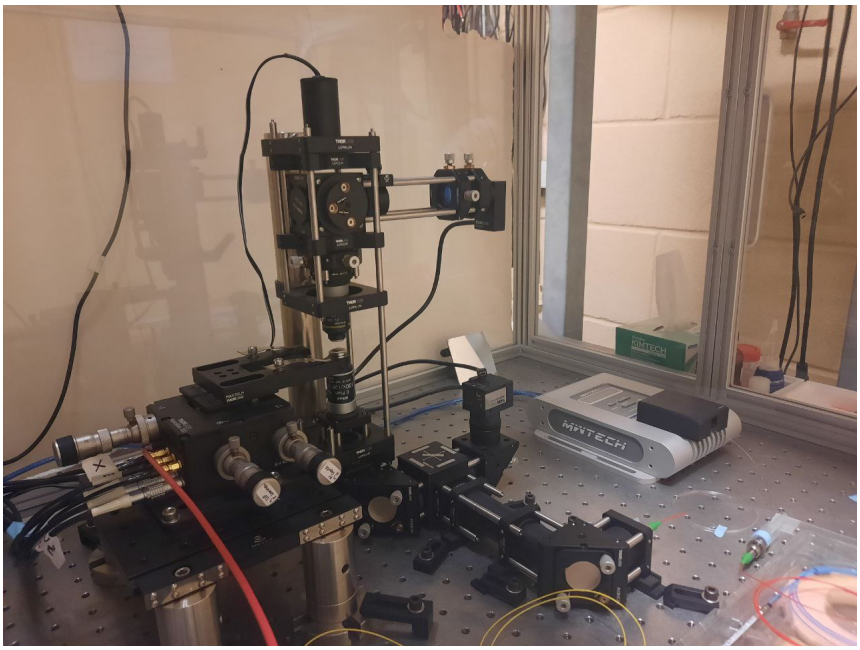

FIGURE 2.4: Our current optical tweezers setup, the Modular Optical Tweezers by Thorlabs.

A fiber coupled laser diode (Lumentum s27-7602-460) of $\lambda = 976nm$ is used as the trapping laser source, which is connected to a single mode optical fiber ($980nm$, SM 980-5.8-125 by Thorlabs) for spatial filtering purposes. The ensuing collimated beam enters the optical path and is then reflected by steering mirrors to a galilean beam expander comprised of anti-reflection coated achromatic doublets with an expansion factor of 3, in order to achieve the maximum filling of the back aperture of the microscope objective (d=10 mm), improving trapping and establishing conjugate planes between the back aperture and the mirrors. The beam then enters the 100X oil immersion objective (E Plan 100x/1.25 Oil, Nikon, and the immersion oil has a refractive index of $\approx$1.5), which focuses the beam onto the sample to generate the trap with a beam spot size of approximately 1.1 μm.

After the beam travels through the sample, it is collimated again by an air condenser lens (Nikon 10X air condenser with a numerical aperture of 0.25) before being directed at dichroic mirrors which aim the incoming light at a quadrant photodetector (PDQ80A by Thorlabs). The detector is positioned at the conjugate back focal plane of the condenser lens, for retrieving information about the particle position using the forward scattered light coming from the sample. To achieve the imaging of the trap center and measure the relative displacement of particles in it, the objective and the condenser lens are placed roughly 7 mm apart. We have also attached an XY cage adjuster with a neutral filter with optical density of OD=0.6, and a 40 mm lens to be able to align the beam with the center of the photodetector with a precision of 1 mm perpendicular to the normal axis and prevent detector saturation. The lens serves to image the back focal plane of the back aperture of the condenser lens onto the detector.

The setup has an additional arm where the light from a LED passes through the sample and the trapping objective and is redirected toward a 1280x1024 color CMOS camera (DCC1240 by Thorlabs) for image acquisition, in its way passing a short pass filter with a cut-off wavelength of 750 nm to prevent saturation and a 200 mm achromatic lens to image the sample plane onto the camera. It is also worth noting that the sample holder is placed in a stage that is connected to piezoelectric engines in cube modules for high precision manipulation of the sample holder. Particle size calculations are performed by determining the relationship between the magnification in the image obtained by the camera and the pixel size. We now detail each of the components of the setup and explore their functions and connections with the rest of the system.

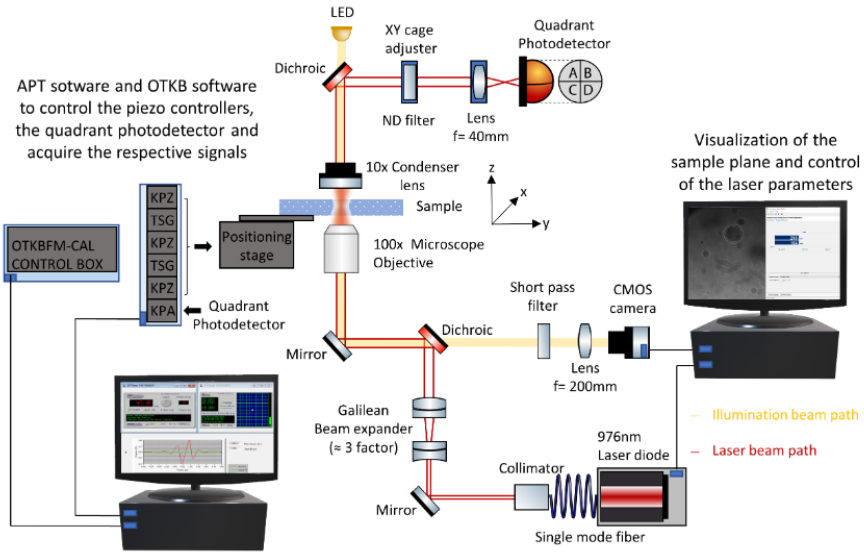

FIGURE 2.5: Schematic of the OT setup, with the components discriminated by function [54].

2.2.1 Stages and Controllers

In addition to the required elements of the optical tweezers setup, it also boasts a stage controlled by three K-cube piezo controllers (KPZ), a positioning system that when a voltage difference is applied, imparts a displacement onto the stage, obtaining a nanometric precision movement, monitored by three T-cube strain gauges (TSG); additionally, a K-cube beam position aligner (KPA) is used to acquire data from the photodetector. These are all connected to a USB Controller Hub and Power Supply device (KCH601), which in turn is connected to the power supply. The hub powers each cube individually and makes accessing the information provided by the cubes possible with a single USB cable, which is very useful for organizational purposes. The K-Cubes and T-cubes operate together to achieve a 3D monitorization of the stage motion and can be controlled in open or closed loop mode. These two distinct operational modes can be summed up by a workflow chart, present in Figure 2.6. The open loop mode functions by applying the desired voltage to the actuator without any later measurement of the actual displacement caused by the piezo, which leads to, as mentioned in the Thorlabs manual, imprecise motions of the stage, albeit being a faster process. This difference stems from the lack of linear function of the piezo cubes past a certain threshold of voltage, losing the sought effect of linear correlation with the input voltage.

On the other hand, the closed loop operation allows for the monitorization of the actual displacement. After the initial voltage application, the appropriate strain gauge

measures the movement of the stage and reports the result back to the piezo device, which then corrects the difference, resulting in a more precise displacement of the stage. The downside of this approach is the time it takes for this feedback loop to end, which can be turned negligible by adding high-speed acquisition systems.

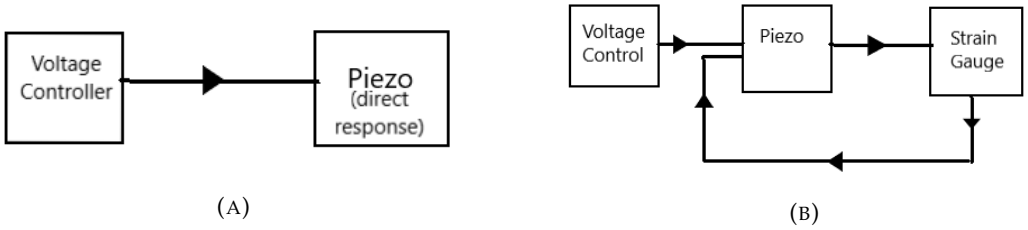

FIGURE 2.6: (A) A schematic of the open loop mode. The voltage is applied to the piezo actuator with no measurement of the actual displacement that has occurred. (B) Closed loop mode. The process has a feedback system for precision displacement.

Through this manner, it becomes possible to move the stage with 20 nm of precision, with a maximum range of 20 μm.

The additional position aligner (KPA) handles the output of the photodetector and allows the visual monitoring of the incoming signals in real time. As well as its counterparts, it possesses a closed loop and open loop mode of operation, mainly for automatic beam centering. However, the KPA has an additional method of operation, the monitor mode. This mode enables the direct tracking of the output signals with a maximum bandwidth of 10000 Hz using a digital acquisition (DAQ) system.

2.2.2 Quadrant Photodetector

The quadrant photodetector is an essential part of the optical tweezers system, as it allows for the accurate position detection of the trapped particle, providing in this way the necessary data for the stiffness and force calculations. Chosen over the traditional position sensing detector, the QPD is a semiconductor photodiode that converts the forward scattered light coming from the sample into measurable photocurrents. This device is divided into 4 segments called quadrants, seen in Figure 2.7, with a gap between them of about 0.1 mm. Throughout this work we have utilized the PDQ80A Quadrant Photodetector by Thorlabs, a pincushion tetra lateral sensor with a peak responsivity of 0.65 (W/A) at 976 nm and a bandwidth of 150 kHz. The apparatus is designed to detect the position of beams with a beam diameter in the [1-3.9] mm range, and has a size of 7.8 mm.

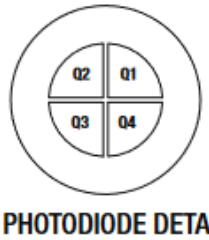

FIGURE 2.7: Schematic of the quadrant photodetector from the specsheet. Quadrants were marked and given a number for identification.

Quadrant photodetectors are very reliable tools for laser position detection, being sensitive to the lateral displacement of the beam and possessing a high temporal and spatial resolution [55], being widely used in scientific works owing to the precise process it undergoes when illuminated. Being the photodiode a p-n junction, whenever light comes into contact with the surface of the detector, if a photon has enough energy, it will eject a electron with a specific energy, per the photoelectric effect, by way of electron-hole pair creation. As a consequence, a very small photocurrent is formed in the photodiode that is proportional to the irradiance of the incident light, occurring in all four segments. These photocurrents are then put through a trans-impedance amplifier to amplify and convert the currents into voltage signals. The output signals can then be obtained through the six pins connected to the photodiode, of which only three pertain to the acquired data. These three pins represent the two positions X and Y, or more accurately, the difference signals, and the total intensity of the incident beam, the SUM signal. These signals are sufficient to locate the beam within the photodetector surface and are obtained using the expressions

$$\begin{aligned} X_{\text{Diff}} &= (Q_2 + Q_3) - (Q_1 + Q_4) \\ Y_{\text{Diff}} &= (Q_1 + Q_2) - (Q_3 + Q_4) \\ SUM &= (Q_1 + Q_2 + Q_3 + Q_4) \end{aligned} \tag{2.16}$$

where Q_i is the voltage measured by the ith quadrant. Evaluating these in the context of Figure 2.7 will yield that the X_{Diff} parameter is the voltage detected on the left side minus the voltage detected on the right side, thus able to resolve any horizontal beam drift from the center. The Y_{Diff} parameter follows the same logic for the vertical direction. The SUM signal is related, as previously stated, to the total intensity, and its main purpose in our analysis is the normalization of the other two signals, so as to obtain the relative drift in both directions. Normalizing the above equations leaves us with:

$$\begin{aligned} X &= \frac{(Q_2 + Q_3) - (Q_1 + Q_4)}{Q_1 + Q_2 + Q_3 + Q_4} \\ Y &= \frac{(Q_1 + Q_2) - (Q_3 + Q_4)}{Q_1 + Q_2 + Q_3 + Q_4} \end{aligned} \tag{2.17}$$

It is clear that these factors equal zero for a perfectly centered beam, since the voltage on each segment would be the same, leading to the canceling out of the numerator on the above equations. It is also easy to see that the positive values of X and Y correspond, respectively, to the right and above the center of the photodetector. After the correct calibrations, we acquire the voltage values for the position of the beam, but it remains essential to retrieve the equivalent displacements for the description of particle motion. As in [54, 56], we assume a linear correlation between the measured voltage and the experienced displacement, which takes the mathematical form of:

$$\langle X \rangle = \langle (V_{QPD} \times S_{QPD}) \rangle \tag{2.18}$$

where X_{QPD} is the axial displacement in length units, V_{QPD} is the voltage detected by the photodetector and S_{QPD} is the calibration factor of the detector, which converts the measured voltage to a distance. In this fashion, we retrieve the necessary information about the particle motion under the trap.

2.2.3 Sample holder

For sample support, it is necessary to take into account the requirements of the optical tweezers. As outlined in [54], reproducibility problems occur when using the manufacturer-provided glass slides with a built-in channel.

Furthermore, the fragile nature of the object and the difficulty in loading samples onto it drove us to build our own sample holder design. The comparatively small working distance of the objective lens led to the conclusion that a very thin glass window was required, with a hole in the middle of the holder for the loading of a coverslip, as is visible in Figure 2.8. Our in-house sample holder design is made using a 3D printer, with free space to house the fluid in order to have sufficient conditions for trapping.

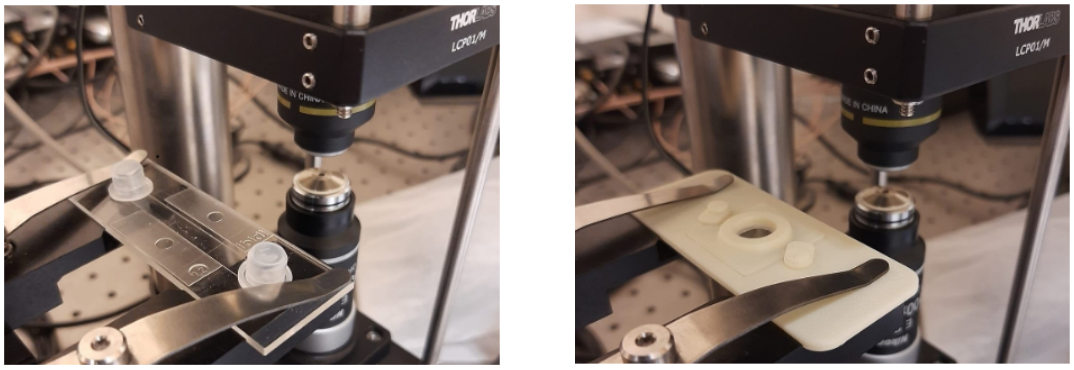

(A) (B)

FIGURE 2.8: (A) In this picture, the manufacturer provided glass slide, impractical for our needs of the system [54] (B) Designed sample holder for the system. The coverslip holds the fluid in its confines, together with the walls of the holder.

2.2.4 Concluding Remarks

In this chapter, we looked at theoretical explanations of optical trapping events within various optical limits, as well as the driving engines and interactions of optical tweezers. The analysis methods employed in this work are also outlined and discussed in terms of their robustness and speed. In addition, an overall view of the experimental setup is provided, with special emphasis on the different components and their functions.

Chapter 3

Characterization of the experimental setup

After introducing the theoretical principles of OT and describing our experimental setup, this chapter dedicates to preliminary characterization studies and methodologies to ensure proper and reproducible experiments. For this purpose, we first present results for the characterization of our beam shape and output power of the trapping laser. Besides, we also present the methodology and typical results for stiffness calculations, not only validating the methodology but also introducing tools that will play a role later on this disseration for the classification algorithm. Finally, we also design a sample preparation protocol which shall be followed to ensure reproducible results.

3.1 Trapping Laser characterization

In order to ensure optimal trapping conditions, we performed some calibrations on the incident laser beam, analyzing the output beam shape and power.

3.1.1 Beam shape

In order to determine the beam shape at the output of our laser, we first used the Knife Edge Method [57] according to the methods detailed in the ISO 11146, to obtain the M^2 and the beam divergence θ_0 parameters. Later, with the acquisition of the Thorlabs BP209-IR/M - Dual Scanning Slit Beam Profiler equipment, we repeated the measurements in a more reliable manner, using a computer to perform the analysis with the software Thorlabs Beam.

Axis(Power)	M^2	θ_0
X (50 mA)	1.06	0.800º
Y (50 mA)	1.04	0.899º
X (150 mA)	1.07	0.807º
Y (150 mA)	1.04	0.904º
X (200 mA)	1.07	0.804º
Y (200 mA)	1.03	0.909º
X (300 mA)	1.07	0.803º
Y (300 mA)	1.03	0.909º

TABLE 3.1: M^2 and θ_0 measurements for various TEC currents.

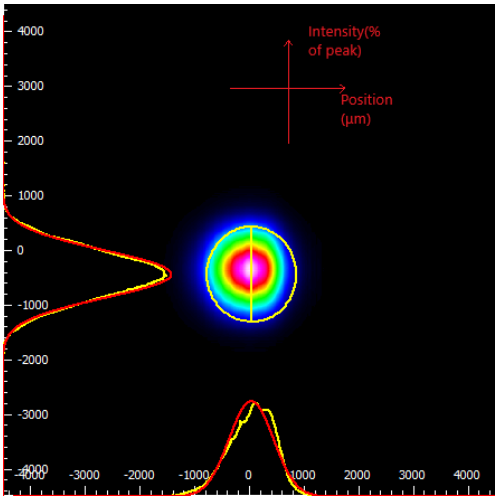

FIGURE 3.1: 2D reconstruction of the intensity map of the beam and the respective intensity profile in each direction.

The results of this experiment were documented on Table 3.1 and Figure 3.1. Both parameters remained constant throughout the measurements and at reasonable values for our requirements, meaning $M^2 \approx 1$, which implies the beam is very close to an ideal gaussian. Although high M^2 and divergence trapping are possible [58], it demands a high degree of focusing and implies a non-gaussian trapping potential, which becomes impractical in our setup.

The optical fiber integrity was evaluated as well, to guarantee maximum output to the optical system. For such a task, a video microscope fiber inspector (CI-1000 Fiber Optic Connector Inspector) was used and any problematic zones were repaired through splicing.

3.1.2 Output Power

Since the laser driver only allows the control of the current passing through the diode, a precise relationship between this current and the output power at the end of the optical fiber must be attained. Thus, studies were conducted to determine the exact relationship between the current provided to the thermoelectric cooler (TEC) of the laser and the output power of the beam after passing through the optical fiber, to better assess the power incident on the sample plane, and consequently the examined particles. For this end, we used the laser coupled with the chosen optical fiber (Lumentum s27-7602-460 laser

and SM 980-5.8-125 optical fiber by Thorlabs), and a power meter to determine the incident power (PM100D by Thorlabs with a thermal power sensor head, model S302C). A schematic of the experiment is visible below in Figure 3.2, while the results are visible in Figure 3.3.

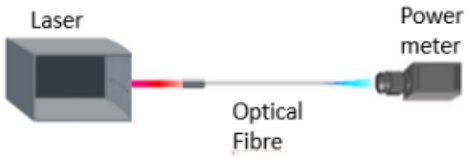

FIGURE 3.2: Schematic of the output studies experimental setup.

The power meter was kept quite close to the optical fiber in order to deal with the laser divergence. We concluded that, as expected, the power increases linearly with the current for the tested range. However, we note that the measured power is substantially lower compared to the laser display, which confirms the need for this accurate calibration.

Finally, the alignment of the optical path of the system was also thoroughly examined, as it is an integral part of the trapping phenomenon.

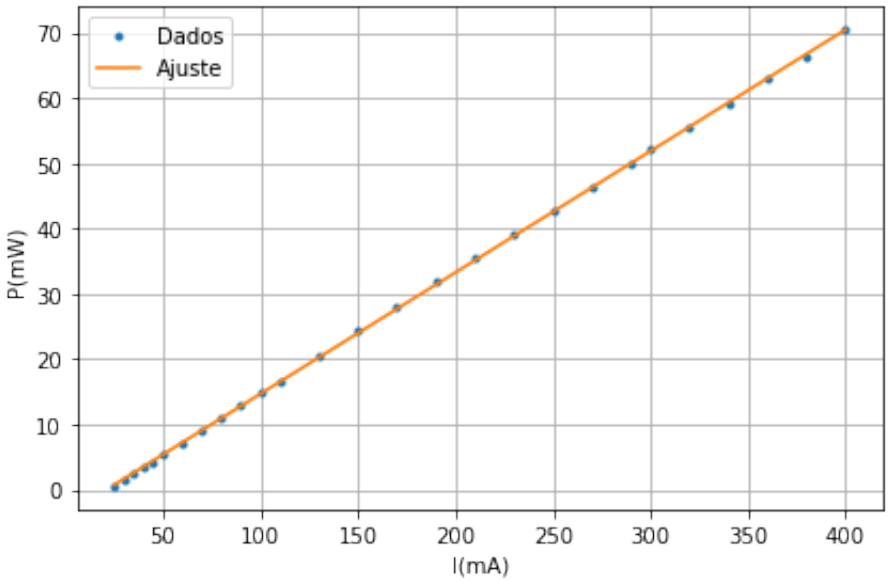

FIGURE 3.3: Current vs Power plot of the data obtained in the output studies.

3.1.3 Force and Stiffness Computations

After characterizing the trapping laser, we advanced to the validation and characterization of the optical trapping procedure. To this aim, we now describe in detail some

specific measurements for force and stiffness calculations, in accordance with the procedures stated earlier in the document. All analysis scripts were executed using the Python programming language, a powerful and open-source tool, which will also allow easy integration with the control software presented in the next chapter of this dissertation.

3.1.3.1 Equipartition Method

In order to calculate the trap stiffness with the equipartition method, it is necessary to calculate the variance of the retrieved signal. In this specific scenario, the required ensemble average calculation by the equipartition theorem is replaced with a time average, which is valid under the ergodic condition [53].

For that end, we acquire the forward scattered signal in the quadrant photodetector for a total of 30 seconds, and divide the retrieved data into 500 ms segments, as seen in Figure 3.4, which will constitute smaller time intervals to avoid drifts due to laser heating and associated convection currents. After this subdivision, the X, Y and SUM signals are separated, to handle them in convenient manner. The X and Y signals are normalized using the SUM signal to account for the light intensity that reaches the QPD. Moreover, it is necessary, as mentioned previously, to convert the voltage signal coming from the detector to position dimensions. These factors were calculated in reference [54] using the stuck bead method. Succeeding this step, we calculate the stiffness for every segment, as can be seen in Figure 3.5, according to Equation 2.14, using as reference temperature the constant value 295.15 K.

In order to obtain the stiffness coefficient, a mean is calculated on all the attained coefficients from the segments, which brings down the uncertainty of the measurement by the well-known $\sqrt{N}$ [59], where N is the number of points acquired. Typical results are presented in Figure 3.6.

3.1.3.2 Power Spectral Density Method

For the PSD method, the same segment division is applied, albeit this time, the power spectrum is calculated using the *signal.welch* from the package *scipy*. As mentioned previously, this spectrum is expected to be, theoretically, of a Lorentzian form, a function we the use to fit the attained data, a representation of which can be found in Figure 3.7.

A low pass filter is applied to the incoming signal at about 1132.8 Hz and a high pass filter at about 78.1 Hz, making this method resistant to ambient noise such as room

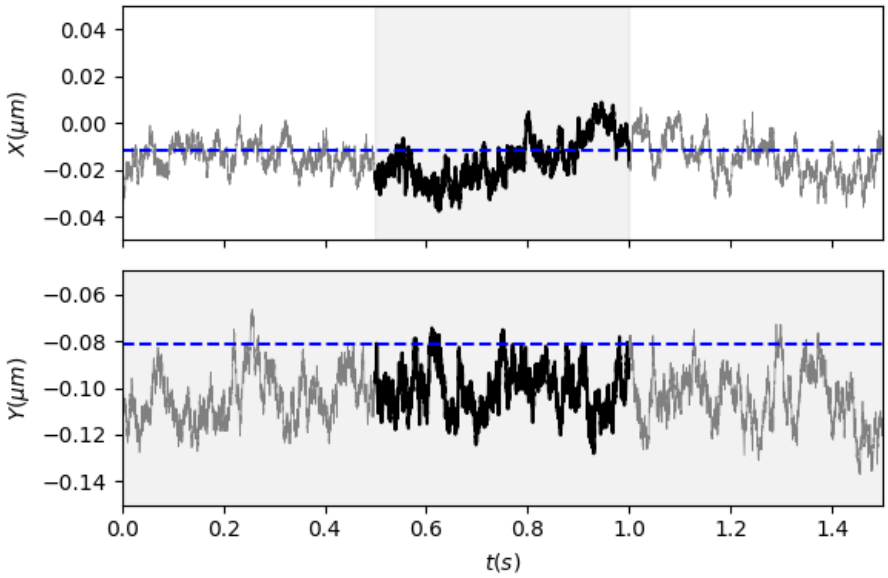

FIGURE 3.4: Retrieved signals from a trapped particle with the quadrant photodetector. The X and Y signals are normalized to the SUM signal in order to account for the variations in total intensity hitting the detector. The dotted line is the calculated mean of the signal and the highlighted portion is a 0.5 s segment of the total retrieved segment.

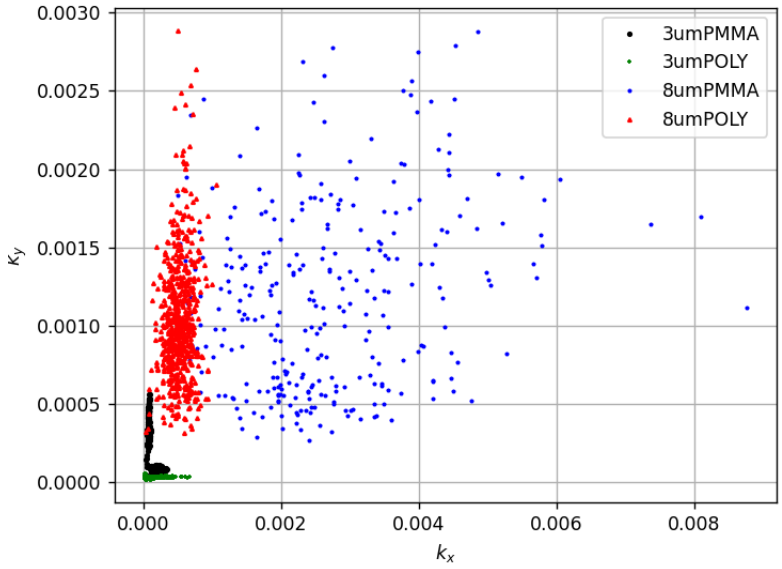

FIGURE 3.5: Representation of stiffness coefficients of several particles taken from the mentioned segments.

illumination or rapidly oscillating phenomena. Fitting the computed one sided power spectral density to Equation 2.15 enables the determination of not only the stiffness of the trap, but also the corner frequency and the diffusion constant. Again, typical results can be found in Figure 3.6, which align with the results obtained for the equipartition method.

Particle type	Particle size(μm)	StiffnessX(N/m)	StiffnessY(N/m)
Polystyrene microspheres	3 μm	$(1.01 \pm 0.04) \times 10^{-6}$	$(2.80 \pm 0.03) \times 10^{-5}$
	4 μm	$(1.9 \pm 0.1) \times 10^{-4}$	$(1.65 \pm 0.07) \times 10^{-4}$
	8 μm	$(5.19 \pm 0.06) \times 10^{-4}$	$(1.03 \pm 0.02) \times 10^{-3}$
PMMA microspheres	3 μm	$(1.39 \pm 0.03) \times 10^{-4}$	$(2.87 \pm 0.07) \times 10^{-4}$
	8 μm	$(2.73 \pm 0.05) \times 10^{-3}$	$(1.15 \pm 0.03) \times 10^{-3}$

FIGURE 3.6: Typical trap stiffness coefficients obtained for some of the used materials using the equipartition theorem method [54].

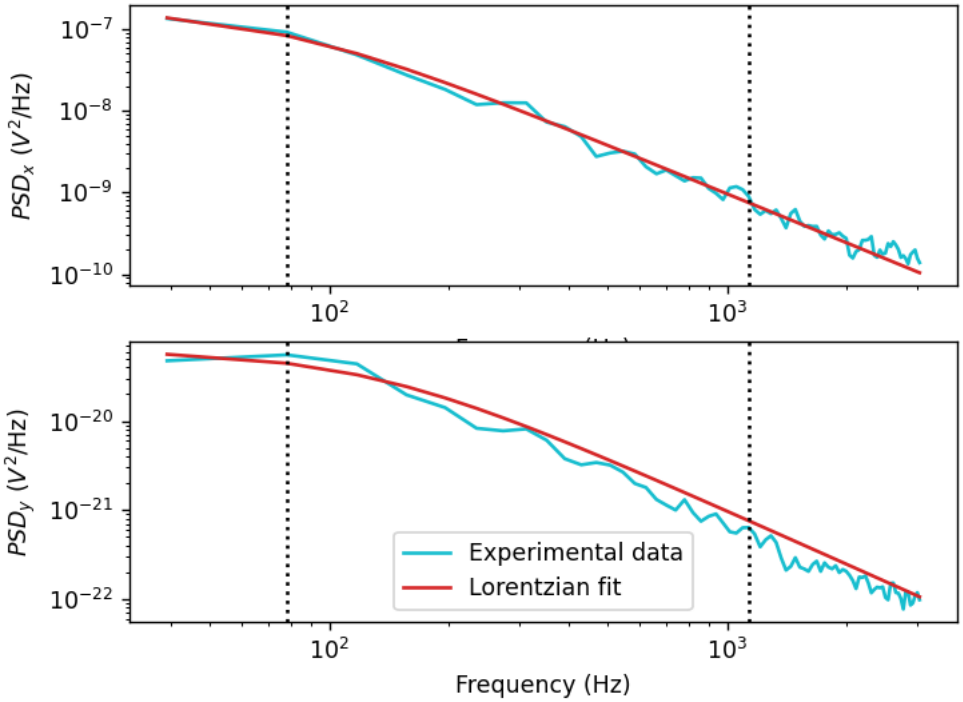

FIGURE 3.7: Power spectral density of a segment of the output data in logarithmic scale, complete with a curve fit using the least squares method, computationally calculated with the *curve_fit* function of the package *scipy*.

3.2 Protocol for Sample Preparation and Data Acquisition

Sample preparation is a crucial step in every experimental procedure, and thus requires a detailed protocol for maintaining the consistency of the measurement methodology. As the optical trapping phenomenon demands the analysis of a particle inserted in a medium, free of external forces besides the ones imposed by the incident beam, a careful method of sample production was outlined. As for the materials used in the collected

data, a mix of organic and non-organic materials were chosen so as to have a diverse set of particles for analysis and classification (in Table 3.2), in this way testing the developed methods with a wide array of samples.

Particle Identification	Particle Size (μm)	Organic
Polyestyrene microspheres	3.0 4.0 8.0	No
PMMA microspheres	3.0 8.0	No
Carboxy PMMA Beads	5.0	No
Carboxy PMMA beads bound to a Streptavidin protein	4.8	No
Tetraselmis Suecica	≈5.0	Yes
Tetraselmis sp.	≈3.0	Yes

TABLE 3.2: Materials used throughout this work, a mix of organic and non-organic particles for performance rating.

The capabilities of the technique and the classification procedure are also being studied regarding the size of the particles, since the selected particles have different sizes. In order to obtain an acceptable classifier tool, it is imperative that the protocol differentiates dissimilar sized particles.

3.2.1 Preparation of Non-organic Materials

Several materials are needed: two types of micro-pipettes, the 1-10 μL (P10 model by GILSON) and the 200-1000 μL (P1000 model by GILSON), plastic tips for both, a glass beaker, a plastic pipette for later use and an eppendorf. For the preparation itself, we start by using the beaker to hold the chosen medium, which in this work will be primarily deionized water (n=1.3270 @976 nm). Then, after inserting the eppendorf in the proper support, the P1000 micro-pipette with the respective tip is used to measure the volume of water necessary for the solution. We then introduce the desired particles in the same fashion, albeit with the P10 micro-pipette, into the eppendorf as well. In most cases, these solutions have a total volume of 1.05 mL, or more specifically, 1 mL of solvent and 50 μL of solute. For the loading of the sample onto the coverslip surface of the sample holder,

we use a plastic pipette to retrieve a few droplets of the prepared solution. Two prepared solutions are visible in Figure 3.8.

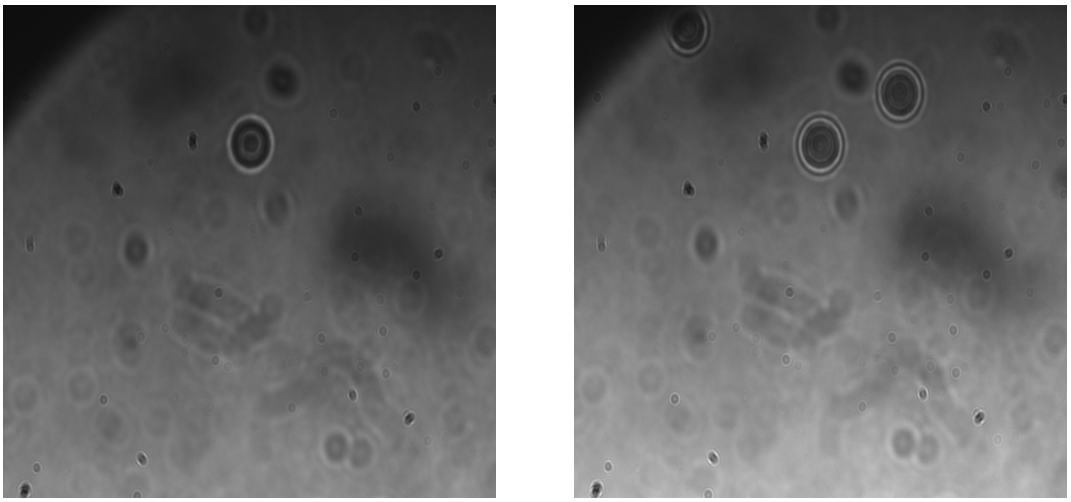

(A) (B)

FIGURE 3.8: (A) A 3 μm PMMA particle suspended in a deionized water solution (B) A 4 μm Polystyrene particle. Both images were obtained with the setup's camera.

3.2.2 Algae preparation

For the organic specimens that were selected, a different sample preparation protocol was developed for purposes of non-contamination of the algae by external bacteria. Furthermore, as the algae were not yet mature upon their acquisition, a feeding regiment was established as well to make sure they reached the adult stage of development. The aforementioned regime consisted of keeping the algae in a room with dimmed light, away from direct exposure to the sun, and in a saline solution (f/2 Guillard, 5‰:28‰) in a sealed test tube. Once a day, the bottle in which they were held was shaken in order to disperse the algae throughout the solution.

In order to acquire a sample from the test tube, we use an alcohol burner and a glass pipette so as to not contaminate the algae solution. While the burner is on, we retrieve a sample from the test tube with the pipette in a careful fashion, avoiding when possible hitting the walls of the tube. After usage, the pipette and the opening of the tube are passed through the flame for sterilization, which when completed prompts the resealing of the tube. Two examples can be seen in Figure 3.9.

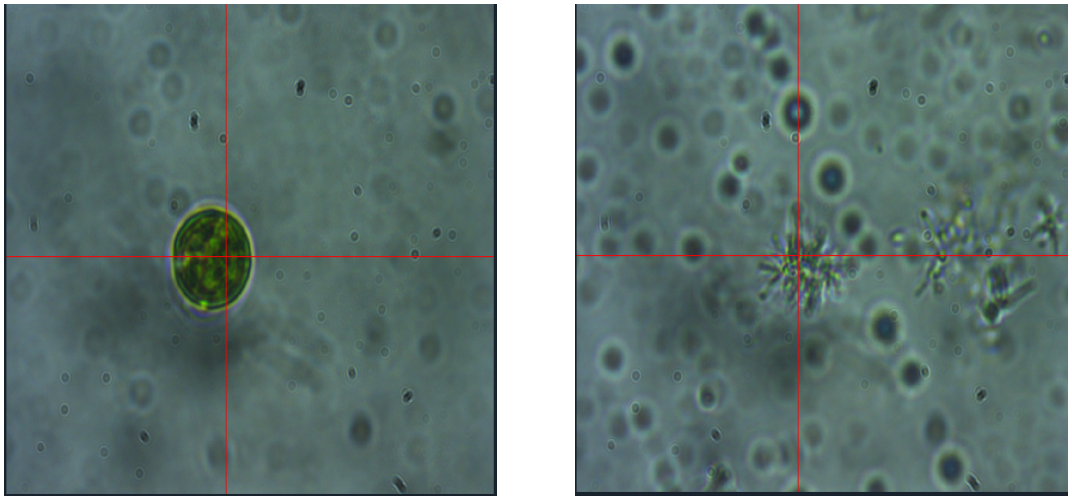

(A) (B)

FIGURE 3.9: (A) A *Tetraselmis suecica* algae, with a clear view of the silica skeleton it's known for possessing (B) A *Tetraselmis sp.* algae, possessing flagella.

3.3 Concluding Remarks

In this chapter, we have explored the calibrations performed for the setup described in the previous chapter, with an additional description of the sample preparation of the various organic or non-organic particles used in this work. Along with these assessments, a study of the application of the analytical methods on the gathered data and information regarding the quadrant photodetector output data are supplied.

Chapter 4

Automation and Graphical User Interface

After following the protocol for trapping particles several times, using the commercial software and specifications, it becomes apparent that the conjunction of the utilized programs was impractical and at times difficult to work with. Indeed, controlling laser, stages, camera and quadrant photodetector acquisition require four distinct softwares from different vendors. This fact established a need for a single platform where the individual elements of the system could be easily manipulated, incorporating the necessary controls for trapping, force/stiffness calculations, classification, and presented as a Graphical User Interface (GUI) for our optical tweezers system, allowing to ease the learning curve of users at the entry level of expertise.

In this chapter, we describe this endeavour that had the purpose of combining all the controllable trapping components synergistically into one application, facilitating not only the process of using the setup, but also the addition of new elements as needed.

4.1 General structure of the code

The code is organized into several structured layers, which are stacked according to their function and from lower-level functions to higher-level ones, meaning each layer requires the previous ones to be deployed. These layers range from component drivers to the graphical user interface, which itself has a nested format, as discussed later. A visual schematic of the layering can be seen in Figure 4.1. For a better control of the elements in the system, we were compelled to write drivers for all the components, at times adapting

packages made by the manufacturer or templates from Github, otherwise creating them from the ground up, which is the case for the laser driver. After the conception of this part of the software, the next layer hinges on the control and integration library, which is where some important subroutines like commonly used operations such as obtaining video from the camera or piezo and laser controls are located. This modular and versatile framework allows for the manipulation of the components in a much easier away, aggregating the operations needed for simple use, all the while remaining programmable in the sense of writing unique routines.

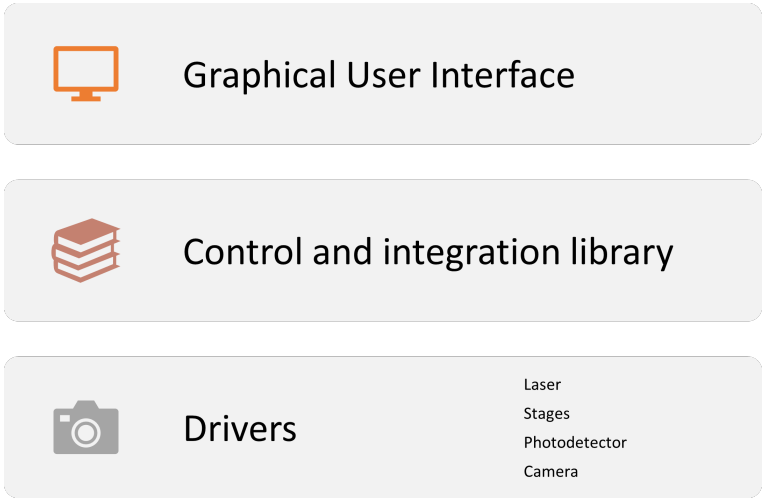

FIGURE 4.1: Layer structure of the interface.

All of the code was written in Python, a powerful yet simple language with a generally great support for hardware drivers, especially for scientific purposes. Also, it was properly documented to allow future users to explore the code at distinct levels of expertise. The actual interface was created using the PyQt5 framework for Python, that is a wrapper of the Qt package, written for the C# programming language.

An important note on the development and deployment of the automation code is that we found that elements can setup communicating with each other but also can work separately, involving completely parallel tasks. Therefore, to develop the most agile framework, we used multi-threading techniques to handle them efficiently. Besides, for operations that competed for the same resource, a queuing system was implemented to make sure all actions were executed, this way turning synchronous events into asynchronous.

4.2 Driver Development

The drivers are at the cornerstones of a system control software, since they interface directly with the hardware and allow it to be manipulated in the designated fashion suitable for the respective goal. Indeed, great care must be taken with these components to ensure that they run as efficiently as possible while still serving the wider objective of being integrated into a multipart system. The following is a quick summary of how the drivers work and the decisions that accompanied their development.

4.2.1 Laser Driver

Controlling the laser is an essential task of the optical tweezers system, and as such, its drivers have a direct impact on the trapping phenomena. This particular laser controller, the MWTech cLDD, already possesses a manufacturer supplied interface, complete with its own drivers and protocols. This software, however, was created in the Java programming language, which does not meet our requirements because its integration with Python is not as efficient as a Python-based driver. Moreover, the actual code used for this interface was not freely available, therefore requiring the drivers to be built from scratch.

The developed drivers follow the Directory Access Protocol (DAP) and the Device Management Protocol (DMP), which establish a data flow schematic between the master device (computer) and the slave device (laser driver). These devices share packets of data continuously communicated through the USB protocol, with a specific format to allow for the efficient use of the information required for the various tasks. This data flow organization is very useful for the control of the driver, since the connection is always open for the reception of packets.

All data exchange transactions occur inside a single communication channel connecting the device ports, implying that supplied data must be ordered by time of request, with the requests are processed in chronological order. For this end, a FIFO (first in first out) queuing system was implemented, since the laser system lacked an internal queue, queries that were made too close together were ignored, a feature that is detrimental to the functioning of the driver. A schematic of the functioning of this driver can be seen in Figures 4.2 and 4.3.

Organizing the requests in this way promotes the change from the possibly synchronous occurrence of incoming requests into an asynchronous operation, without loss of packages.

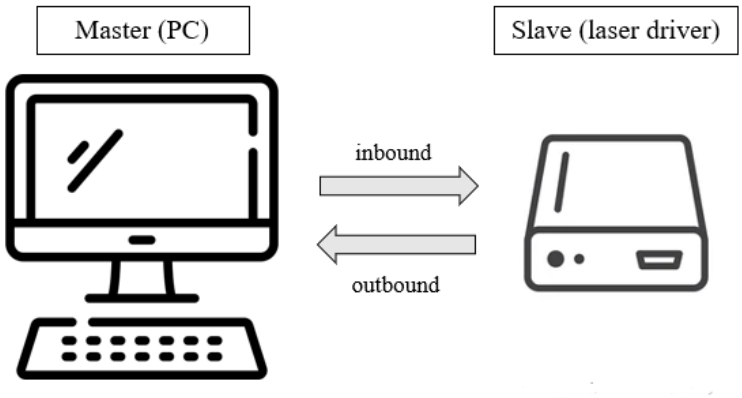

FIGURE 4.2: Master and slave relationship established by the DAP and DMP protocols.

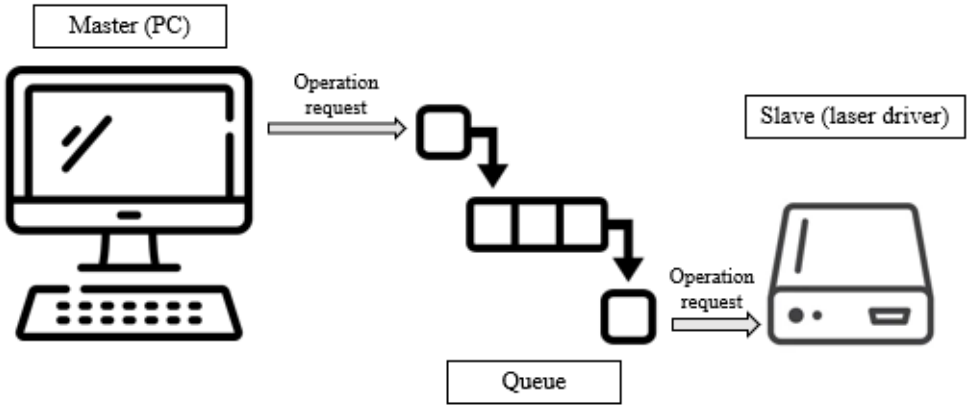

FIGURE 4.3: Queuing system for the update and actions requests, leading to lossless communication between the devices.

Types of requests can be divided into two classes: updates and actions. Actions are sporadic and do not happen in a predictable way. Instead, these requests are sent whenever the need arises. Turning the laser on, off, changing the laser current, etc., all fit within this category, and do not expect any response from the driver (except the action itself) unlike the second type, the updates. These requests serve to monitor the state of the laser, as well as the thermoelectric cooler (TEC) current, power and temperature. They are sent in an orderly fashion, and expect a response from the driver, which are the necessary values. The two types of requests compete for the driver resource, and because the driver is somewhat slow (response per request $\approx$0.1 s), updates are 1.3 seconds apart. This time interval is a compromise between the freedom of requesting actions at will and updates that appropriately portray the system current status.

Finally, when the laser is turned off, the USB connection is immediately terminated,

preventing the driver channel from becoming clogged. This has the benefit of being able to restart the laser with no resource constraints.

4.2.2 Camera drivers

Imaging the sample plane of an optical tweezers setup brings forth the need for a high quality camera, and thus, its control. Driver development for this component was fairly straightforward, in the sense that the program works with a simple multithreading operation that uses the camera to take a snapshot of the image, which is then processed and shown on the interface. The original proposal to this goal was to display a live feed of the camera using the manufacturer-made drivers provided by Thorlabs. However, because Thorlabs did not provide an open source platform for this specific camera, we were obliged to use standard OpenCV camera drivers.

Since we are using external drivers in order to control the camera, its efficiency is suboptimal, as the frame rate suffers from the operations the module requires. Nonetheless, the measured frame rate is around 17 fps, which is adequate for the designated function.

4.2.3 Piezo Actuators Drivers

Piezo actuators are not as essential to the system as OT can work without them if the user manipulate the stages using manual actuators. Yet, driver development for their use prepares the path for further system automation, which is one of the goals of their utilization. Their manufacturer (Thorlabs) has developed an API for the control of the piezo actuators, which allows for the writing of user specific code. However, this platform was made for the C# *.NET* framework, which collides with our Python control system. The proposed solution was to create a wrapper solution around this framework, in this way enabling the use of these functionalities in Python, with the caveat of a slower response time. Since the K-Cubes (KPZ and TSG) can only have one physical connection at a time, a protocol must be made for their use. Whenever their needed, the program connects itself to them via USB connection, performs the necessary actions, and disconnects from the devices, guaranteeing that the resource is free for subsequent uses. A schematic of the process can be seen in Figure 4.4.

The K-Position Aligner behaves in a slightly different manner than its counterparts. Since constant information between the device and the driver must be traded, it connects to the driver when the program starts and only disconnects when the program stops.

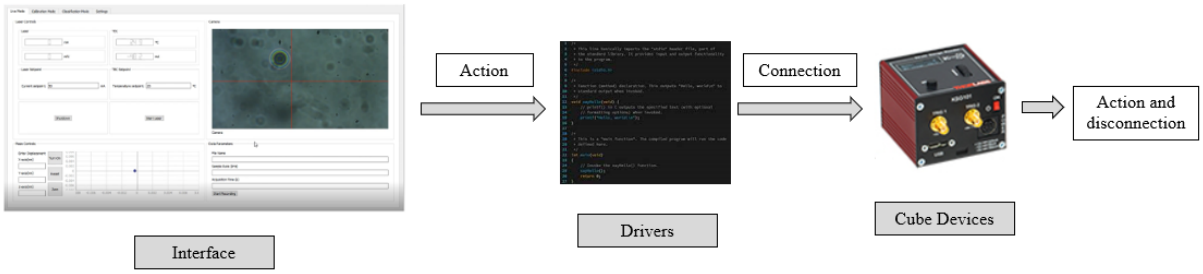

FIGURE 4.4: Schematic of the interaction between the interface and the KPZ and TSG cubes. The drivers connect to the devices only when a request is made by the interface (user). After the cubes perform their duties, they disconnect from the program.

Figure 4.5 shows a diagram of the transmitted data among the different components.The data flows repeatedly between the interface and the KPA, with the drivers functioning as intermediary, mediating the interface requests and the incoming data, thus resulting in a continuous loop with these elements. Because the KPA continuously streams data via the drivers, beam location is monitored in real time, allowing for considerably easier centering and control.

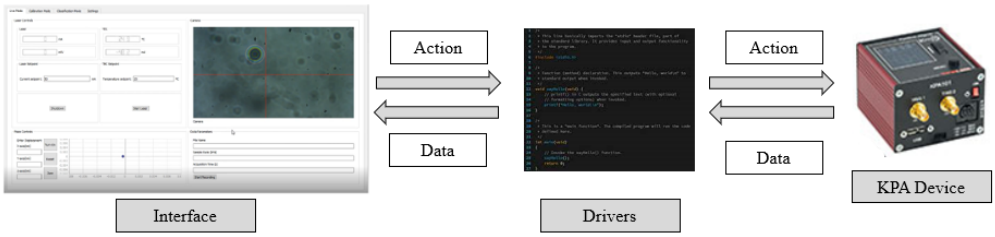

FIGURE 4.5: Schematic of the interaction interface-KPA cube, which is performed in a cyclic fashion while program is active.

4.2.4 Data Acquisition Driver

Finally, we examine the data acquisition drivers, which is a critical component of the program. The data is collected using a National Instruments DAQ device furnished by the setup's manufacturer. Thorlabs, once again, did not create a platform for manipulating this device, forcing us to construct our own libraries. To avoid using LabVIEW, which is a closed source software and does not function well with Python, we built a wrapper for NI instrument control using the package *nidaqmx*. When the data acquisition option is selected, the application collects 500 points at a time and saves them in a file in a more suitable format for our requirements. This intermittent saving was necessary since long period data acquisition functions from the package took up most of the resources of the

program, effectively immobilizing it while the device recorded the necessary data. The answer was to store the data in chunks, with the ideal chunk size discovered through trial to be 500.

4.3 Graphical User Interface

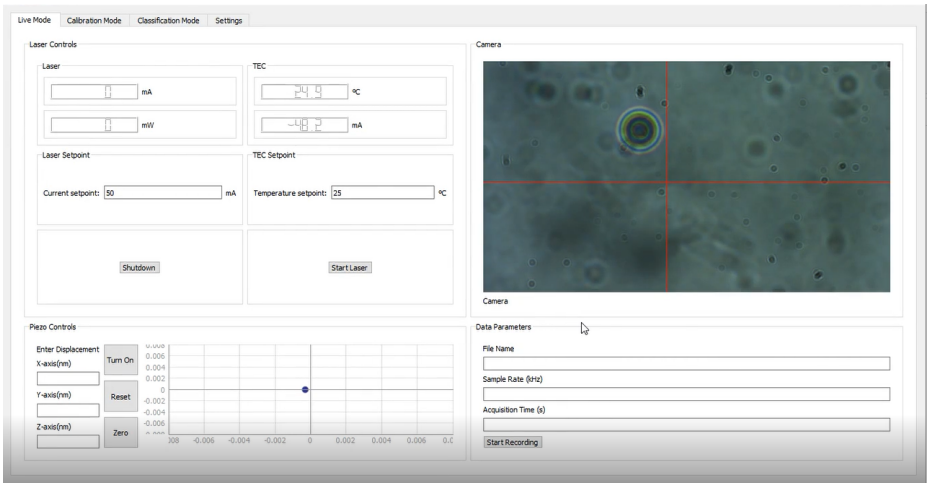

FIGURE 4.6: Live mode tab in the GUI.

A snapshot of the interface developed can be seen in Figure 4.6. As mentioned previously, the GUI is organized into nested components called widgets using PyQt5. The main window contains all the widgets and is able to manipulate all other levels that are inside of it. The built-in functionalities are divided into four tabs for a better user experience: the live mode tab was designed for quick trapping of particles and data acquisitions, and possesses the main controls of the constituents of the system, more specifically laser controls, piezo voltage settings and laser beam alignment monitoring, imaging from the camera feed and a data acquisition widget; the calibration mode, which is designed for force and stiffness calibrations and features a real time display of the incoming data from the detector; the classification mode...; and the Settings tab allow the user to control general settings of the setup.

4.3.1 Live Mode

The live mode is the first window tab of the GUI and, as mentioned in the past section, is designed for quick acquisitions of data. This module allows for an easy manipulation of the OT setup components and divides naturally into four areas, as seen in Figure 4.6. The

laser window enables the control of the laser state, i.e. the turning on and off the laser, as well setting and monitoring the current of the thermoelectric cooler (TEC), with the appropriate displays for these factors. Additionally, it is possible to establish the expected TEC temperature setpoint, which has a built-in alarm system that is triggered whenever the temperature goes above a critical range. For optimal performance, the stated range has been chosen to be 25 ± 0.1 ºC as provided by the laser manufacturer.

FIGURE 4.7: Display of the laser controls, with laser current and temperature setpoint functionalities.

Whenever the alarm system is activated, we design a pop-up message that appears on the screen to alert the user and the laser is shutdown, for safety purposes. The function of the buttons are outlined in Figure 4.7. The state of the laser (Laser current, Laser power, TEC temperature and TEC current) is updated every 1.3 seconds and displayed in the monitors. This slow update time is due to the long response period of the laser controls, and for this reason we also implemented a queuing system to make sure all user requests reached the laser drivers and were executed in the correct order. It is worth noting that the power measurement displayed on the power monitor is not the value the laser controls provide, as this is not an accurate representation of the output power after the optical fiber. Instead, the displayed number is attained by using the parameters calculated on Section 3.1.2, as it is a more accurate depiction of the optical power that reach the particles.

In regards to the camera widget, the image is obtained via several snapshots taken by the camera, instead of video, and presented in the GUI window at a constant rate. This is a departure from the ideal solution, which would be to obtain a live video feed from the camera. However, due to the fact that Thorlabs does not produce drivers for our specific

type of camera, other software was required to access the data, making the video capture capabilities of the camera unavailable. A representation can be seen in Figure 4.8.

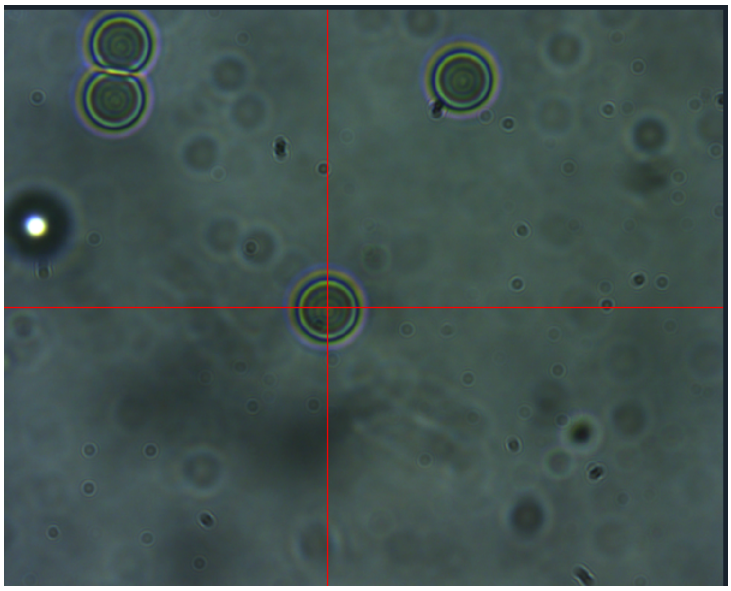

FIGURE 4.8: Display of the camera widget, complete with two red lines detailing the position of the laser spot size to aid in the trapping process.

This live feed operation, like the laser status updates, is working simultaneously with the main GUI window using multithreading capabilities. This implies that they work in tandem with one another and share information when appropriate. The red lines on the image meet on the laser spot size center, and they are drawn manually by trapping a particle and centering the mark in the correct position. As for pixel size, calculations are required to determine the scale of the image and its elements. For the 1280x1028 pixel image the camera produces, we have calculated that 1 pixel equals 5.3 μm. However, for fitting an appropriate size to the widget, the camera feed was reduced to a smaller 640x480 sized image.

The piezo widget controls allow the user to manipulate the piezo actuators and monitor the KPA data in a live setting. For this end, and as mentioned above, we were obligated to write drivers for each of the components, as Thorlabs only designed these to be use in the C# .NET framework. The controls are fairly straight forward: on the left, the manipulation of the piezo actuators. This interactive box allows the user to impart a specific displacement to the stage in the desired direction. After the chosen length is input, pushing the turn on button calculates the appropriate voltage and promptly supplies it to the piezo cubes.

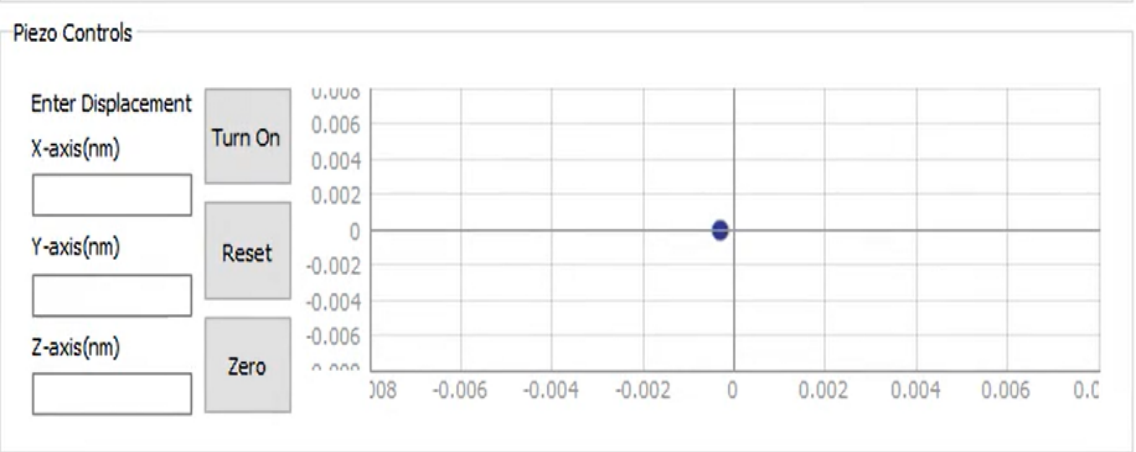

FIGURE 4.9: Piezo controls box displayed. The single point in the chart is the laser spot size position, which is monitored through the QPD.

Other buttons can also be selected, as seen in Figure 4.9, with assorted useful functions. The reset button aims to retract all the voltage supplied to the piezos and return them to their original state, which is the state the actuators were immediately after their powering on. This tool is extremely important in the context of multiple particle tracking, when data from various particles must be collected, and it is necessary to know in which direction the new particles are being gathered. Lastly, the zero functionality is mainly for turning the voltage of a specific piezo cube to zero. In regards to the right side, the graph is a live display of the KPA data, which tracks the laser and the trapped particles. Its primary role is to center the laser, which is accomplished by moving the XY cage adjuster until the dot is as closer to the origin of the graph as possible.

Finally, we also have the data acquisition widget, which serves to retrieve data from the quadrant photodetector for a pre-specified time period at a designated frequency. The controls feature a file name input, as illustrated below in Figure 4.10, which lets the user choose the name of the file containing the data. Data formatting and extension is, however, not an option to customize by the user, as they have a pre-determined shape to fit further analysis scripts.

When the record button is pressed, the widget connects itself to the data acquisition card (USB6212 by National Instruments) and collects its data in 500 sample portions, as the continuous acquisition functionality of the DAQ crashes the application. In all measurements in this work, a 10KHz sample rate was used to collect data of 30 second readings, in this way making sure a full description of the particles movement is captured.

FIGURE 4.10: Data acquisition widget, with input sections for the file name, sample rate and desired acquisition time.

4.3.2 Calibration Mode

The calibration mode tab was created with the purpose of performing calibrations and tests while monitoring the live feed of the output signal. With this in mind, the widget contains two sections: the recording section, which is equal to the one previously described, and the live data graphic depiction. Specific subroutines for the automatic calibration are still in development, based on the stuck bead method [60].

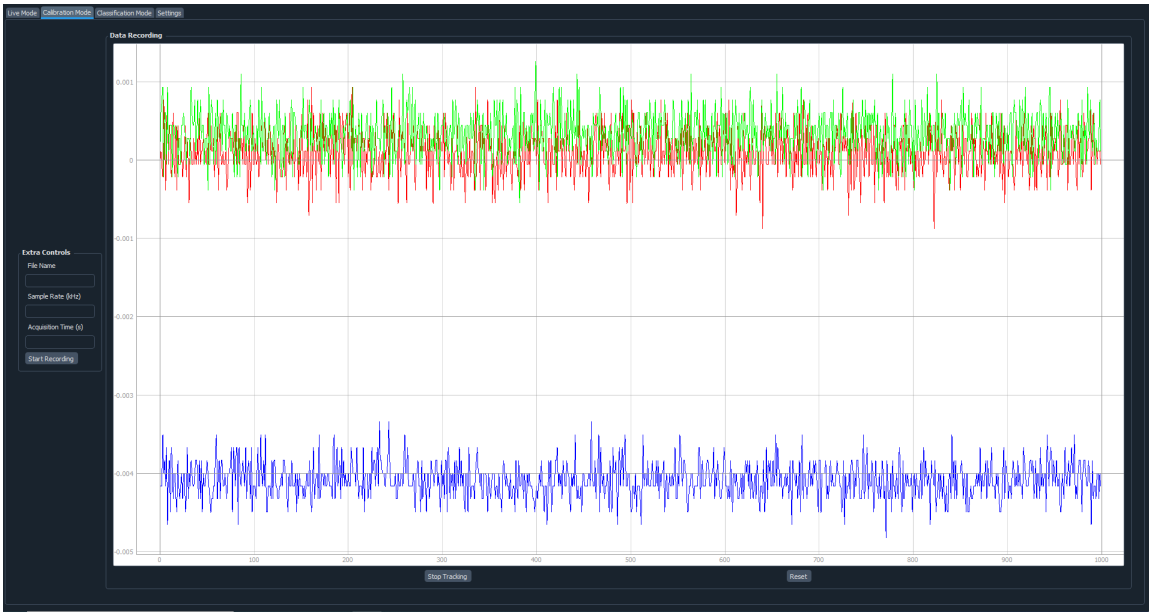

FIGURE 4.11: Calibration mode, which is capable of recording and displaying live data acquisition, a distinct feature that is useful while trapping particles and monitoring laser performance.

This widget can work in tandem with the live mode as well, which is a useful tool to make sure the trapping has occurred and the laser is working properly. Moreover, the live feed of the photodetector data and the recording features work in a completely parallel fashion, so stopping the live feed does not affect the data collection. Once again, we make use of the multithreading capabilities of the PyQt5 framework, allowing for concurrency

in our tasks. A snapshot of the widget is seen in Figure 4.11. This formulation brings several advantages, one of them being that it does not compete for resources against other tasks. The latter implies that when this widget is terminated, it disconnects from the DAQ, freeing up the channels for other operations.

4.4 Additional modules

New tools were built in collaboration with other students in order to accomplish full automation of this optical tweezers setup and more efficient classification approaches, adding modules to the described interface and converting it into a more versatile program. To aid with this goal, an automatic trapping functionality based on image processing techniques was created, potentially contributing to system miniaturization [61]. This area of research is critical because it employs currently available resources to extract more information from samples, with potential applications in optofluidic devices and biochemical sample monitoring. The signal analysis component of the protocol has also improved, with the use of Uniform Manifold Approximation and Projection (UMAP) for dimensionality reduction, replacing PCA, which is a powerful yet slow algorithm [62]. The combination of these efforts helps to solidify the use of optical tweezers in biology and medicine as a viable option for sensor development.

4.5 Concluding Remarks

This chapter describes the graphical user interface that was created to improve the work flow of the optical tweezers system and to facilitate the data collecting process. The program architecture was conveniently discriminated, as well as the connections between all the components of the software. The conjoined research into the development of this interface, more specifically the addition of new modules, is also outlined.

Chapter 5

Live Classification using Forward Scattered Light: from synthetic to biological samples

Using the automation toolbox developed and described in the last section, our OT experimental setup is now equipped to ease data acquisition, analysis, and obtain reliable results in timely manners.

In this chapter, and based on previous works of the research team at Center for Applied Photonics at INESC TEC [39, 40], we attempted the live mode classification of optically trapped particles utilizing OT forward scattered signal. As for the algorithm, the acquired data is first treated in Principal Component space which serves as input for training a machine learning model for classification purposes. The manner of treatment of the data set is outlined in this chapter, before advancing to three case studies involving particles of distinct materials.

5.1 Deploying a classification algorithm

As we have already seen, the forward scattered signal acquired with the quadrant photodetector can be used to characterize the dynamical properties of the trapped particle, in particular in the Fourier domain by taking the Power Spectral density. Therefore, some information that is particle-specific is encoded in its shape, and thus this signal can be used for classification purposes. Yet, instead of feeding a classification machine learning model

directly with this data, one can rely on dimensionality reduction techniques such as Principal Component Analysis (PCA) to speed up the classification process, avoid overfitting problems, and bypass some measurement noise.

Thus, in order to classify the trapped particles, the collected forward scattered signal is first put through a pre-processing protocol that uses PCA, helping to visualize the data in a projection axis that accentuates the differences and similarities between the data points. Essentially, this machine learning algorithm finds the direction/components that best explain the variance of the dataset. The next step is to represent the data according to these directions, performing a normal change of basis operation. A representation of this process can be found in Figure 5.1. The data spread out in space, and points can then be classified based on their position in relation to other points. As can be seen, a very useful property of this method is the data dimensionality reduction that occurs when using the algorithm, which reduces the data space to the number of dimensions equaling the number of components used.

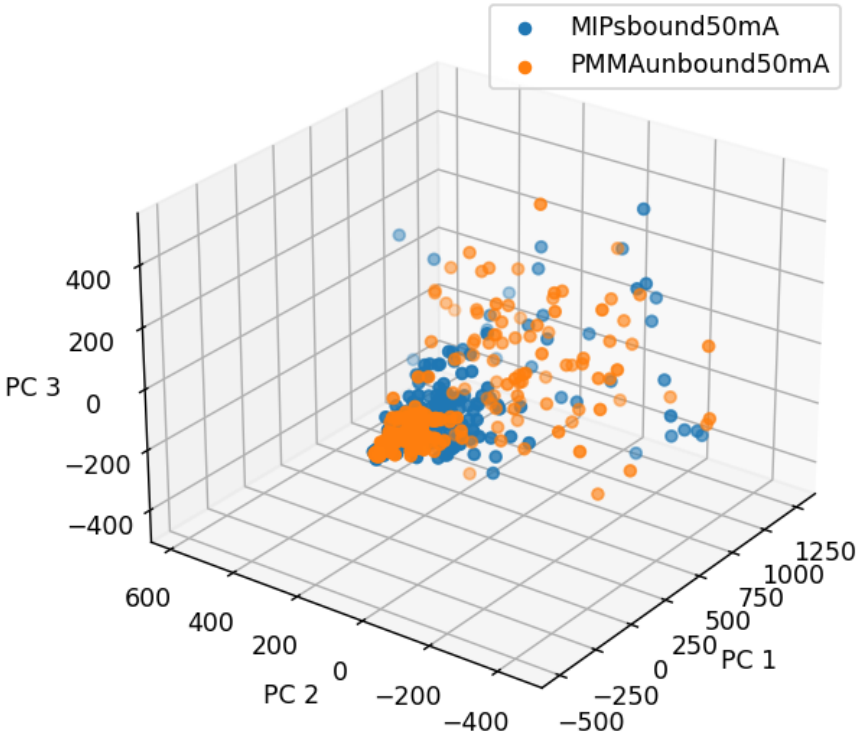

FIGURE 5.1: X component of data points represented in the principal components. The 3D graphic displays the calculated directions that accentuates the differences and similarities of data collected from bound and unbound PMMA beads.

In our pre-processing protocol, only the first 3 principal components were calculated and kept as the new features to be used. This choice is explained by the calculation of the

information gained from the addition of a component, analysis which is represented in Figure 5.2. The graph contains the Explained Variance Ratio (EVR) information, which is the percentage of variance that is attributed to each component added. We can see that the gains associated with adding a fourth component are minimal, and may add detrimental noise to the dataset. From this point on, the algorithms we develop perform operations in this space, as the yielded results are superior to classification in normal k space, as in Figure 3.5.

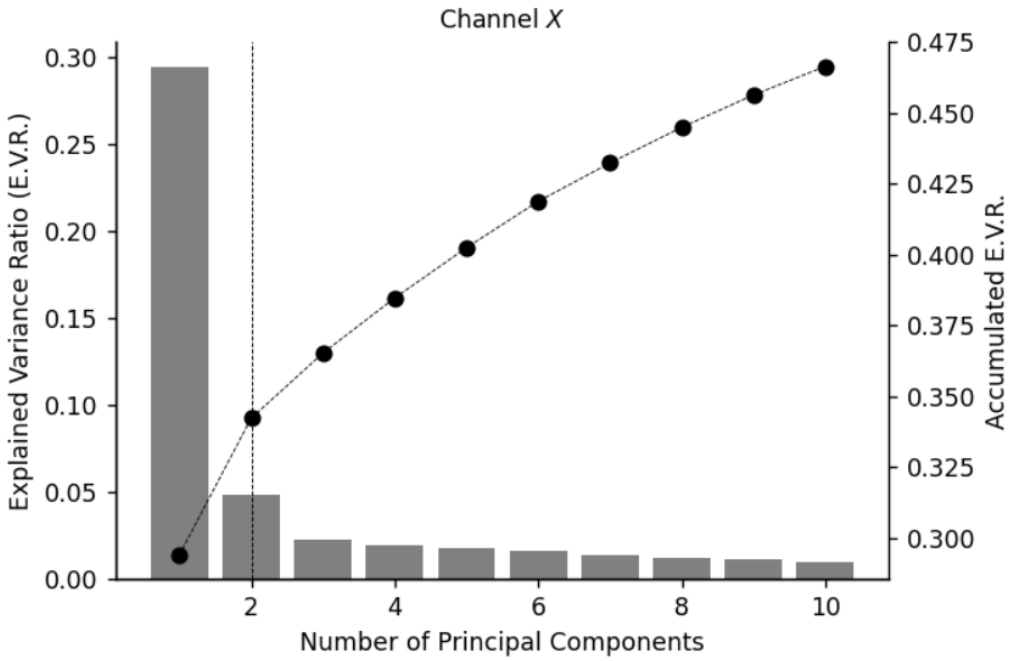

FIGURE 5.2: Explained Variance Ration (EVR) for the X direction data. The returns that are obtained after the 3rd component are minimal compared to the computation workload it carries.

For the creation and training of the actual classifier, we use a wide array of machine learning methods, with varying results. However, the one that has shown most promise in conjunction with the PSD data in PCA space is K-Nearest Neighbour. This algorithm distills down to the extraction of features from a data set by way of assigning a neighborhood of K points to each analyzed point and based on these extracted features, having them vote on what the identification of the particle is by plurality. More voting neighbors provide a better representation of the data and therefore yield better results, although it also carries a bigger computational task, as the assigning of a neighborhood to each particle is a heavy task to perform information-wise.

On the other hand, having many neighbors voting can also cause classifier issues as the model gives importance to data that is located very far away from the specific point

that is being studied. In order to soften the votes from distant points, a weighted voting method based on distance can be applied, albeit many points can sway the vote in the same fashion as before.

5.2 Experimental Results

The development of this approach has the ultimate goal of being employed in a wide range of scenarios, demonstrating the procedure's adaptability. To that purpose, we developed three case studies to evaluate the method's performance. The first case study intends to test the approach with a set of synthetic particles, mostly to demonstrate the classifier's capabilities. The second case study will determine if Carboxy PMMA beads are bound or unbound to a Streptavidin-Biotin combination. These particles are molecular imprinted polymers (MIPs), which are molecules that bind to a specific predetermined protein. These findings provide a proof of concept for identifying MIPs utilizing an optical tweezers technique. Finally, we aim to distinguish between two species of micro-algae, *Tetraselmis suecica* and *Tetraselmis sp.*. This test is meant to evaluate the performance of the setup using biological samples, which is an important phase in the development of a biological/medical identification equipment. We also provide an analysis of the results we obtained, asserting its success or failure.

Regarding the training strategy, we perform a 6-fold cross validation operation to acquire a more accurate depiction of the model performance. In an effort to train and test our model, data separation is required so as to prevent the model from testing an already learned data point and obtaining good results that are not a true classification attempt, biasing the performance analysis. Dividing the data set only once poses a problem as well, since the chosen test data could perform better or worse than the actual model by mere coincidence or a particularly good train set. Hence, one possible solution is to vary the train/test group within the set and average the results. This method is called cross-validation, and since we perform this exchange six times, it becomes 6-fold.

The results are displayed in a normalized confusion matrix, reporting in this way the percentage of guesses that a class of particle was guessed to be part of versus its true label, as visible in Figure 5.3. This matrix rates the performance of the model in an easy and visual fashion, to obtain immediate information about the classification outcome. Although this method is already a good representation of the model performance-wise, we also utilize other important metrics such as the mean success rate, the best result in

terms of percentage, and the worst result, the latter being a very important metric in the determination of success since the standard deviation of the results could be high, with a relatively acceptable mean success rate. The results are normalized horizontally to unity, for a more intuitive description of the results.

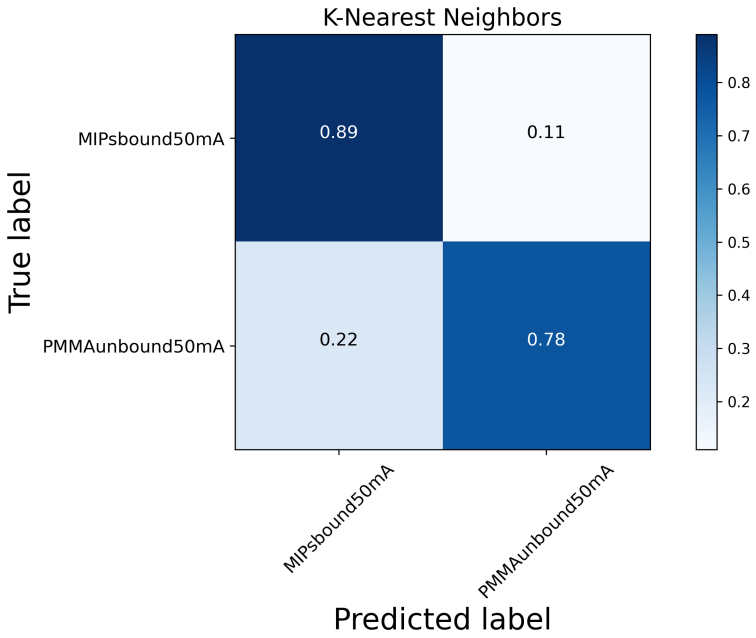

FIGURE 5.3: Normalized confusion matrix outlining the results of a model created using K- Nearest Neighbor.

5.3 Case study 1: synthetic particles

For the first case study we considered a set of synthetic samples already used in previous works [63] and consisting of PS and PMMA particles of distinct sizes. Several particles were chosen and measured with the goal of testing the veracity of the above laid protocols for the classification of a sample set. All the sample were prepared in an aqueous solution (deionized water, n=1.3270 @976 nm) using the protocol outlined in Section 3.2, with the materials present in Table 3.2. Each sample was acquired for 30 seconds at a sample rate of 10 kHz, with 10 acquisitions per material/size pair. The results can be seen in Figure 5.4.

The mean success rate of the classifier model based on the gathered data is about 64.75%, with a best result of 95.38% and a worst result of 38.34%. This disparity in results is not optimal, however, due to the variety of the data set and the relatively limited number of acquisitions per particle, it is conceivable that the procedure has the capacity

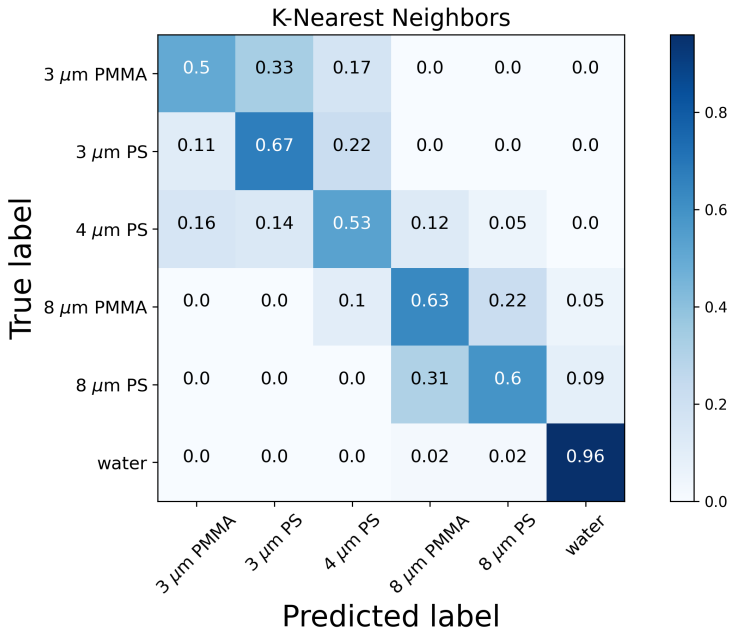

FIGURE 5.4: Classification of a synthetic particle set using K-Nearest Neighbor. Results are less than optimal, but given the diversity of the set, the classifier appears to have the potential to differentiate between particles.

to distinguish between the given particles. Further examinations of the findings indicate that particles with considerable size differences are rarely confused with each other.

Different combinations of machine learning methods and pre processing techniques for the output signal were tested in an effort to determine the best strategy for the classification of particles and interesting results were also found when utilizing the Fast Fourier Transform (FFT) of the output signal and a Random Forest algorithm for classification. Noteworthy results were also found when using the inverse of the power spectral density function.

5.4 Case study 2: Molecular Imprinted Polymer Identification

As already stated earlier in the document, one of the foci of this work is the classification and identification of molecular imprinted polymers. Thus the objective of this second case study is to test the capacity of OT to discern MIP bound and unbound states relative to their target protein. For this, we establish a proof of concept for the use of our tool on micron sized MIPs by way of using Carboxy PMMA beads of the same size, bound or unbound to a streptavidin protein. This protein has a particularly high affinity to biotin, also known as vitamin B7, which is a vitamin that is involved in metabolic processes in

humans and other organisms [64]. This relationship mimics the behavior of actual MIPs when bound to their respective protein. As a result, the molecules we wish to analyze can be naturally replaced by them.

Using the protocol outlined in Chapter 3.2, we collect the detector output signal while trapping the intended particles for 30 seconds at a rate of 10 kHz and a laser current of 50 mA, collecting data for 10 different particles of each type. The signal is then processed using the strategy previously outlined and a classifier is created, trained, and tested using the methods detailed on Chapter 5, with 500 ms segments. The results are displayed in Figure 5.5 in a normalized confusion matrix form, where it is visible that we obtained an average success rate of 82.3%, with a best classification score of 99.4% and a worst result of 44.4%.

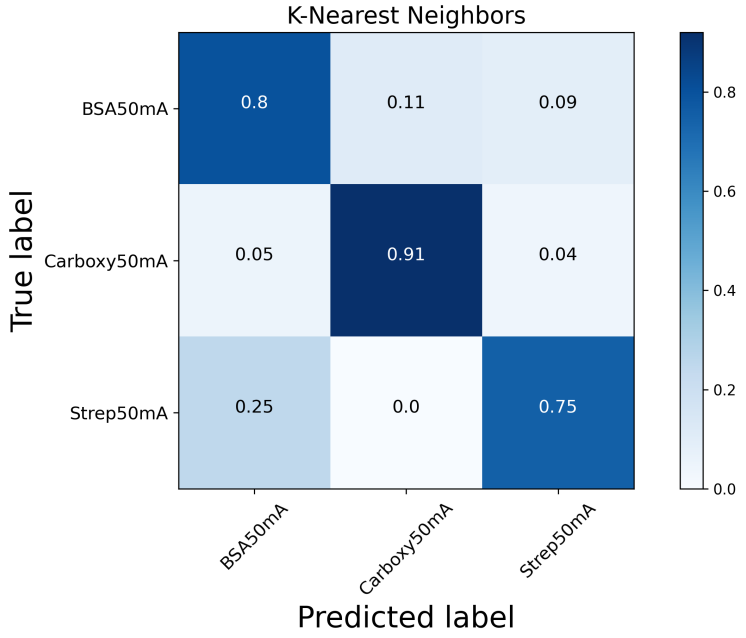

FIGURE 5.5: Obtained results for the classification of Carboxy PMMA beads bound or unbound to a streptavidin protein, which itself could be bound or unbound to a biotin protein.

Further analysis of the results shows that the classifier has its biggest hardship discerning the biotin-streptavidin complex from the streptavidin unbound beads. Although the results are hampered by this lack of precision, given that the difference in the size of the additional complexity is in the nanometric range, these findings give us confidence in the technique we are using to handle the categorization problem we are facing.

5.5 Case study 3: Micro-algae Analysis

In addition to MIPs, we hope to detect live organisms in order to sketch out the prospect of cell classification. For this end, we have chosen a *Tetraselmis suecica* and a *Tetraselmis sp.* micro algae. *Tetraselmis suecica* is a marine algae that is widely utilized in aquaculture as rotifer foodstock. This organism's vivid green hue is owed to chloroplasts holding chlorophyll and being infused with a silica skeleton (see Figure 3.9a). *Tetraselmis sp.* is a species of the genus *Tetraselmis* found in Póvoa de Varzim that has chloroplasts and flagella in its constitution, similarly to the known *Tetraselmis jejuensis* algae.

The results of this case study shed light on the use of the developed classification tool in a biological context, which proves to be useful not only in medicine, but also other fields of natural science. The aforementioned protocol is once again used for these measurements, as 10 collections were taken from each algae at a sample rate of 10 kHz for 30 seconds. The result are visible in Figure 5.6.

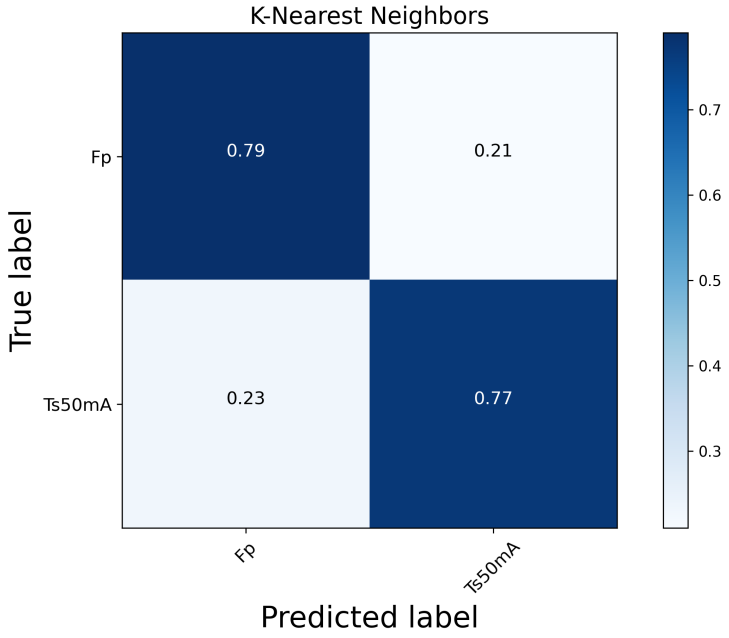

FIGURE 5.6: Classification results for the algae identification study.

We were able to obtain an overall classification success rate of 77.83%, with a best result of 100% and a worst result of 47.5%. These results are somewhat acceptable, albeit showing room for improvement. One possible reason for the underwhelming performance of the classifier stems from the orientation of the algae when trapped. The forward scattered light that collides with the detector contains the information of the particle's

movement in the XY plane, a plane that is parallel to the detector's sensor screen. This indicates that the acquired signal follows the 2D light projection of the 3D particle it is now tracking. Because algae are not symmetrical, position monitoring becomes less reliable because rotational movement is possible when there is no change in spatial location. This rotation, shown in Figure 5.7, regulates the amount of radiation that travels through the sample, thereby registering as movement when it is not actually occurring.

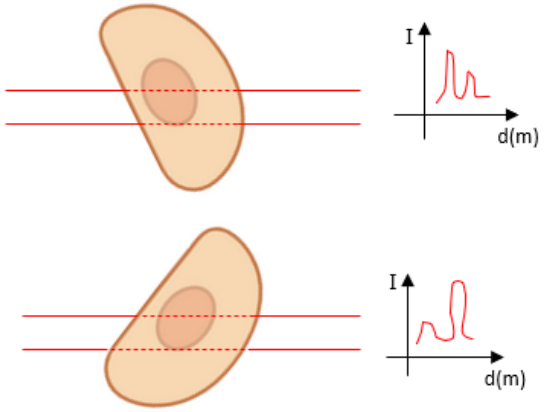

FIGURE 5.7: Rotation affects the signal that reaches the quadrant photodetector, which in turn changes the current produced in each quadrant. Because the photodetector calculates positions through subtraction of voltage in each quadrant, it can be inferred that it would register a movement with this rotation.

Full electromagnetic calculations using Maxwell's tensor are required to calculate the exact scattering effects of the incoming radiation when the geometry of trapped particles is taken into account. T-matrix methods were created for this purpose in order to estimate the scattering effects of light and determine the important quantities of optical trapping. There have been several attempts to investigate a non-spherical shape for trapped particles [65], particularly in simulations of specimens under optical tweezers.

5.6 Concluding Remarks

We discussed the classification protocols created throughout the document that handle the forward scattered light signal described in the previous chapter. We also show some preliminary results that serve as proof of concept for the developed classifier using synthetic particles. Additionally, we have reported the obtained results of the classifier performance in the two case studies proposed in the outline, providing an analysis of the results and possible explanations for the successes or failures of the models, the results being visible

in Table 5.1. The results point toward the possibility of the use of this methodology in all three of the tested environments, whether as a particle classification tool in the case of the molecular imprinted polymers, or a cataloging instrument in the case of the algae.

Classifier Type	**Mean**	**Best**	**Worst**
Synthetic	64.75%	95.38%	38.34%
MIPs	82.3%	99.4%	44.4%
Micro-algae	77.83%	100%	47.5%

TABLE 5.1: Results table for the case studies, complete with the mean success rate, the best and the worst classification results.

Chapter 6

Conclusion and Prospective Work

With this dissertation, we set out to investigate the potential applications of a conventional optical tweezers setup as a tool for biomedical diagnosis. To accomplish this, we deployed a live classification tool based on the assumption that distinct particles with different constituents behave differently while caught under the optical tweezers laser beam. A quadrant photodetector is used to assess the forward scattered light from the confined particles, treating the output data through the appropriate analysis methods and constructing the classifying predictive models with machine learning algorithms.

Beginning with a description of the physical principles of the trapping phenomenon in the two major optical limits, we proceed to provide a detailed explanation of the equipartition and power spectral density methods, which allow for force/stiffness computations, which are at the heart of the classification tool. In addition, an overview of the experimental setup is supplied, along with a description of the main components and their purposes. Furthermore, we describe the system calibrations and sample preparation techniques for organic and non-organic materials. The collected data is then utilized to train and evaluate the previously mentioned categorization method.

Following the setup's characterization, we take a close look at the constructed graphical user interface for the optical tweezers system. In this section, we examine the many layers of the program and their respective responsibilities, beginning with the thought process behind the construction of the component drivers and finishing with a tour of the interface's functions. The purpose of this effort was to make the data collecting procedure easier for novice users while also allowing advanced personnel to write specific subroutines for their needs.

With this knowledge, we progress to describe the classification process, beginning with the development of models that identify particles based on their optical properties under the trapping mechanism. We detail the output data pre-processing technique before discussing the use of Principal Component Analysis in Fourier space, which allows the data to be represented in the directions that most magnify its variance, pulling data points closer together if they have comparable features and vice versa. We also provide early findings for the identification of 3 mum PMMA, 3 mum PS, 4 mum PS, 8 mum PMMA, and 8 mum PS, with a relative success rate of 64.75 %, with a best result of 95.38% and a worst result of 38.34%, arguing for the potential of the model as a particle classifier.

Then, the classifier is tested in case study conditions, using Carboxy PMMA beads that could be bound or unbound to a streptavidin protein. This protein has a very high affinity to biotin, also known as vitamin B7, and their interaction mimics the bonding reactions that occur in molecular imprinted polymers (MIPs), which are our main object of study. For this undertaking, we obtained an overall success rate 82.3%, with a best classification score of 99.4% and a worst result of 44.4%. This establishes a proof of concept for the classifier's use in the molecular imprinted polymers, furthering our objective of developing this technique for biomedical use. Moreover, we provide a new tool for the classification of micro algae, exploring the protocol as a cataloging methodology. We obtained an overall success rate of 83%, with a best result of 100% and a worst result of 47.5%.

In summary, the obtained results validate our initial hypothesis that the optical tweezers setup, accompanied by the developed classification procedure, are capable to discriminate several types of particles in a plethora of contexts, such as organic and non-organic particles, proving its versatility and utility in scientific areas, Furthermore, we can infer its use in the development of biomedical sensors and diagnostic tools, with the possibility of combination with other instruments, to create a sensor fusion approach to screening methods in medical technology, being of utmost importance in the field of biomedical science.

6.1 Prospective Work

As a result of the dissertation's constrained timeline, we were unable to follow various areas of research that were interesting in their own right. Their implications for this work are important for the main objective, thus they are worthy of a brief discussion.

One proposed modification to the setup is the employment of a spatial light modulator (SLM) to regulate the light intensity in the sample plane, hence boosting particle entrapment. The spatial light modulator's capacity to project light in a precise pattern allows for experimentation with a holographic optical tweezers configuration, the benefits of which are succinctly outlined in Chapter 1. One of the attractive features of this technique is the possible use of non-gaussian laser beam, such as Laguerre-Gaussian beams, that could improve the classification and trapping process. This technique is also capable of producing multiple traps, which could be finely tuned to suit our identification needs. Trap stiffness coefficients for non-spherical specimens with the trapping of an *E. Coli* bacteria in a given orientation have been determined in some studies in this subject [66]. Direction, and even trajectory dependent trapping could help solve the problem outlined in Section 5.5. Furthermore, its nanometric spatial resolution is sufficient for the trapping of molecular imprinted polymers, indicating promise for a sensor based on this technology.

Finally, we plan to add a Raman spectroscopy component to the optical tweezers setup for a sensor fusion approach, obtaining the well-known Raman Tweezers configuration. The setup, which is widely used in the biology/medicine sensor development fields, is capable of combining the optical properties determination of the optical trapping phenomenon with the biochemical information provided by the Raman spectroscopy system, undoubtedly assisting in particle classification and identification. Furthermore, both methods are non-invasive, which is critical for biological sensors. Results obtained with the Raman Tweezers apparatus of the classification of colorectal cancer cells using machine learning algorithms yielded promising results [25], indicating a possible new generation of optical sensor based cancer screening procedures, allowing in this fashion a much faster detection process in the oncology field.

Appendix A

Experimental Methods and results

A.1 Fast Fourier Transform (FFT) based results for preliminary testing

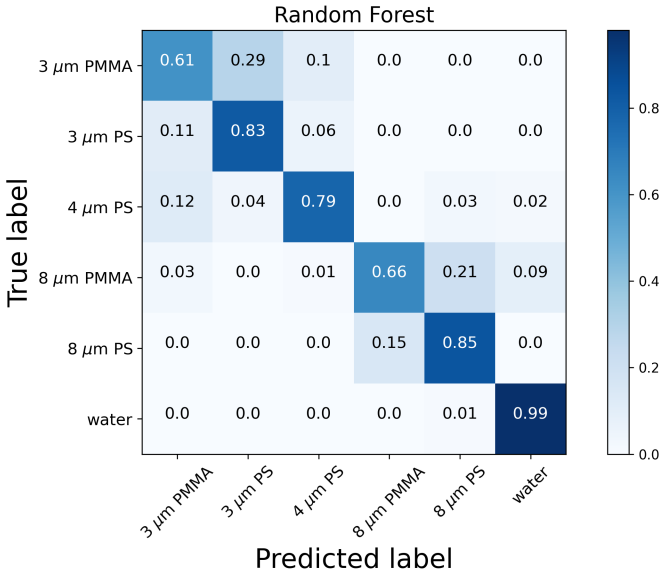

FIGURE A.1: FFT based results using the Random Forest algorithm.

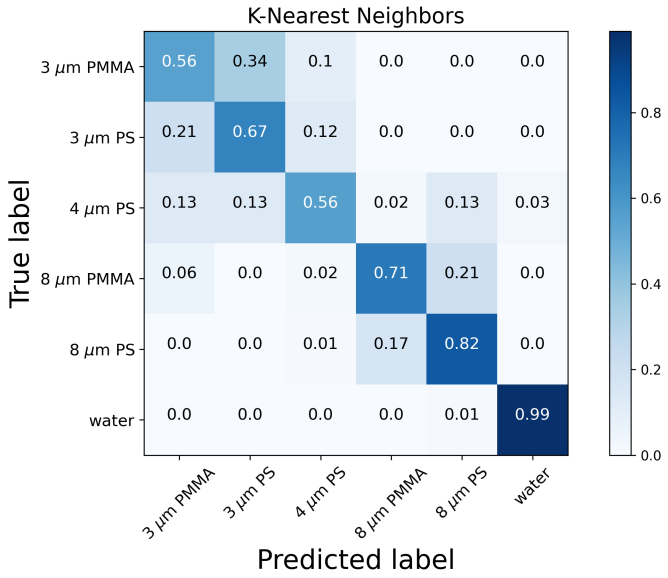

FIGURE A.2: FFT based results using the K-Nearest Neighbor algorithm.

A.2 Back Focal Plane method

The back focal plane approach to the placing of the optical components allows for the imaging of the sample plane in the detector, requiring a very precise configuration of the employed lenses. For this end, the focal plane of the inverted microscope objective has to meet the focal plane of the condenser lens, obtaining in this way a collimated beam after passing through the condenser.

Considering the optical elements in the detection arm of the setup, a set of distances was chosen while taking into account the available space, as seen in Figure A.3. To produce an optimal spot size on the detector's surface, the appropriate distances were selected, being displayed in Table A.1:

Symbol	Value
s_a+ BPA	6.245 cm
s_b	8 cm
$s_0 = s_a + s_b$	14.245 cm
f	4 cm

TABLE A.1: Chosen values for the relative distances for the detection arm.

With these variables, the required distance for the focusing of the incoming light is given by the well-known thin lens equation:

$$\frac{1}{f} = \frac{1}{s_o} + \frac{1}{s_i} \tag{A.1}$$

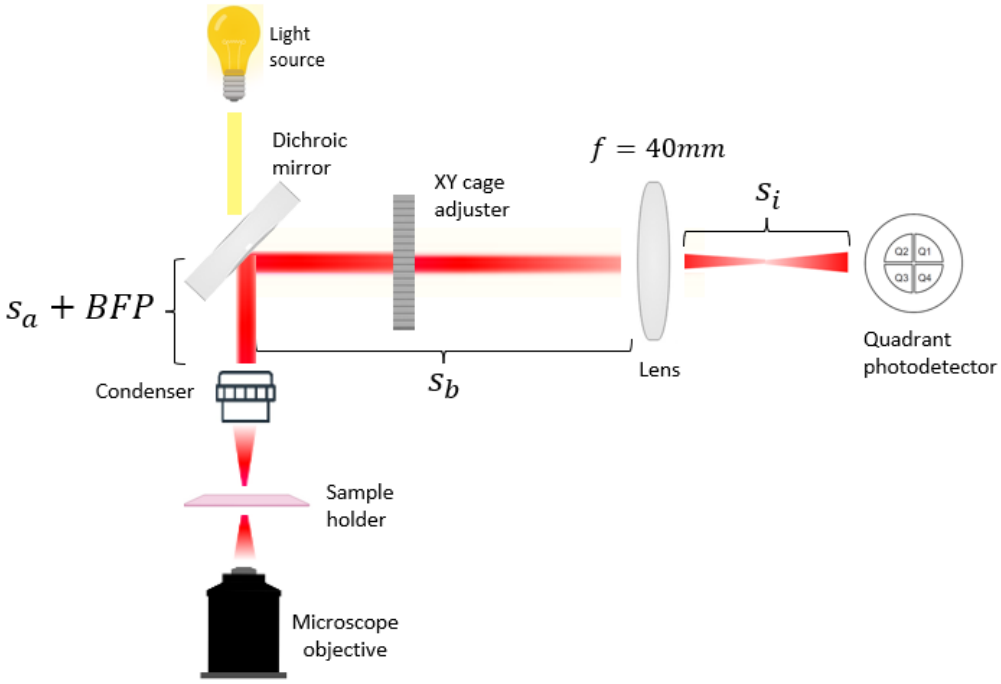

FIGURE A.3: Schematic of the detection arm.

where the aforementioned variables are represented in Figure A.3, s_i being the image distance from the lens. Performing the calculations, we obtain the result of $s_i = 5.5617$ cm. As for the spot size, geometrical optics gives us that the transverse magnification of a bundle of rays originating from an image and passing through a lens will be by a factor obtained by the following equation:

$$M = -\frac{s_i}{s_o} = \frac{h_i}{h_o} \tag{A.2}$$

where h_i is the image size and h_o is the original size of the image. As a consequence of this magnification, the original beam, which shares its width with the aperture of the condenser, being approximately 8 mm wide, becomes smaller in size, with a calculated height of 3.084 mm. This expected height is, according to the quadrant photodetector's specification sheet, the optimal spot size for the beam.

Bibliography

[1] A. Ashkin, "Acceleration and trapping of particles by radiation pressure," *Physical Review Letters*, vol. 24, no. 4, p. 156–159, 1970.

[2] A. Ashkin, J. M. Dziedzic, J. E. Bjorkholm, and S. Chu, "Observation of a single-beam gradient force optical trap for dielectric particles," *Optics Letters*, vol. 11, no. 5, p. 288, 1986.

[3] A. Ashkin, J. Dziedzic, and T. Yamane, "Optical trapping and manipulation of single cells using infrared laser beams," *Nature*, vol. 330, no. 6150, p. 769—771, 1987.

[4] A. Ashkin, K. Schütze, J. Dziedzic, U. Euteneuer, and M. Schliwa, "Force generation of organelle transport measured in vivo by an infrared laser trap," *Nature*, vol. 348, no. 6299, p. 346—348, November 1990.

[5] C. Lafratta, "Optical tweezers for medical diagnostics," *Analytical and bioanalytical chemistry*, vol. 405, 04 2013.

[6] H. Tan, H. Huiqian, L. Huang, and K. Qian, "Plasmonic tweezers for optical manipulation and biomedical applications," *The Analyst*, vol. 145, 07 2020.

[7] X. Xie, X. Wang, C. Min, H. Ma, Y. Yuan, Z. Zhou, Y. Zhang, J. Bu, and X. Yuan, "Single-particle trapping and dynamic manipulation with holographic optical surface-wave tweezers," *Photon. Res.*, vol. 10, no. 1, pp. 166–173, Jan 2022.

[8] J. Jiao, A. A. Rebane, L. Ma, and Y. Zhang, "Single-molecule protein folding experiments using high-precision optical tweezers," in *Optical Tweezers*, 2017, pp. 357–390.

[9] C. Bustamante, L. Alexander, K. Maciuba, and C. Kaiser, "Single-molecule studies of protein folding with optical tweezers," vol. 89, pp. 443–470, 06 2020.

[10] B. Sun, Y. Roichman, and D. Grier, "Theory of holographic optical trapping," *Optics express*, vol. 16, pp. 15 765–76, 10 2008.

[11] D. G. Grier and Y. Roichman, "Holographic optical trapping," *Appl. Opt.*, vol. 45, no. 5, pp. 880–887, Feb 2006.

[12] J. Gieseler, J. R. Gomez-Solano, A. Magazzù, I. P. Castillo, L. P. García, M. Gironella-Torrent, X. Viader-Godoy, F. Ritort, G. Pesce, A. V. Arzola, K. Volke-Sepúlveda, and G. Volpe, "Optical tweezers — from calibration to applications: a tutorial," *Adv. Opt. Photon.*, vol. 13, no. 1, pp. 74–241, Mar 2021.

[13] C. Ti, Y. Shen, M. T. H. Thanh, Q. Wen, and Y. Liu, "Reliable and mobile all-fiber modular optical tweezers," *Scientific Reports*, vol. 10, 2020.

[14] X. Zhao, N. Zhao, Y. Shi, H. Xin, and B. Li, "Optical fiber tweezers: A versatile tool for optical trapping and manipulation," *Micromachines*, vol. 11, no. 2, 2020.

[15] A. Constable, J. Kim, J. Mervis, F. Zarinetchi, and M. Prentiss, "Demonstration of a fiber-optical light-force trap," *Opt. Lett.*, vol. 18, no. 21, pp. 1867–1869, Nov 1993.

[16] A. Rohrbach and E. H. K. Stelzer, "Optical trapping of dielectric particles in arbitrary fields," *J. Opt. Soc. Am. A*, vol. 18, no. 4, pp. 839–853, Apr 2001.

[17] K. Taguchi, K. Atsuta, T. Nakata, and M. Ikeda, "Levitation of a microscopic object using plural optical fibers," *Optics Communications*, vol. 176, pp. 43–47, 03 2000.

[18] H. Xin, R. Xu, and B. Li, "Optical trapping, driving and arrangement of particles using a tapered fibre probe," *Scientific reports*, vol. 2, no. 1, pp. 1–8, 2012.

[19] X. Li and H. Xin, "Optical fiber tweezers for the assembly of living photonic probes," in *Fiber Optics*, G. Huerta-Cuellar, Ed. Rijeka: IntechOpen, 2021, ch. 5. [Online]. Available: https://doi.org/10.5772/intechopen.98845

[20] K. TAGUCHI, R. KIDO, and Y. MIZUTA, "Metal coated chemically etched fiber probe for single cell manipulation and isolation," *Journal of the Japan Society of Applied Electromagnetics and Mechanics*, vol. 23, no. 3, pp. 595–600, 2015.

[21] D. G. Kotsifaki and S. N. Chormaic, "Plasmonic optical tweezers based on nanostructures: fundamentals, advances and prospects," *Nanophotonics*, vol. 8, no. 7, pp. 1227–1245, 2019.

[22] J. Paiva, P. Jorge, A. R. Silva Rodrigues Ribeiro, M. Balmaña, D. Campos, S. Mereiter, C. Jin, N. Karlsson, P. Sampaio, C. Reis, and J. P. Cunha, "ilof: An intelligent lab on fiber approach for human cancer single-cell type identification," *Scientific Reports*, vol. 10, 02 2020.

[23] K. C. Neuman and A. Nagy, "Single-molecule force spectroscopy: optical tweezers, magnetic tweezers and atomic force microscopy," *Nature Methods*, vol. 5, pp. 491–505, 2008.

[24] S. Smith, Y. Cui, and C. Bustamante, "Optical-trap force transducer that operates by direct measurement of light momentum," vol. 361, pp. 134–62, 02 2003.

[25] F. Zheng, K. Chen, and Y. Qin, "Sensitivity map of laser tweezers Raman spectroscopy for single-cell analysis of colorectal cancer," *Journal of Biomedical Optics*, vol. 12, no. 3, p. 034002, 2007.

[26] R. M. Robertson-Anderson, "Optical tweezers microrheology: From the basics to advanced techniques and applications," *ACS Macro Letters*, vol. 7, no. 8, pp. 968–975, 2018.

[27] G. Pesce, A. C. D. Luca, G. Rusciano, P. A. Netti, S. Fusco, and A. Sasso, "Microrheology of complex fluids using optical tweezers: a comparison with macrorheological measurements," *Journal of Optics A: Pure and Applied Optics*, vol. 11, no. 3, p. 034016, jan 2009.

[28] B. Cichocki and U. Felderhof, "Diffusion of brownian particles with hydrodynamic interaction and hard core repulsion," *The Journal of Chemical Physics*, vol. 94, pp. 556–562, 01 1991.

[29] S. Paladugu, A. Callegari, Y. Tuna, L. Barth, S. Dietrich, A. Gambassi, and G. Volpe, "Nonadditivity of critical casimir forces," *Nature Communications*, vol. 7, 2016.

[30] L. Zaidouny, T. Bohlein, R. Roth, and C. Bechinger, "Light-induced phase transitions of colloidal monolayers with crystalline order," *Soft Matter*, vol. 9, pp. 9230–9236, 2013.

[31] A. Yethiraj, "Tunable colloids: control of colloidal phase transitions with tunable interactions," *Soft Matter*, vol. 3, pp. 1099–1115, 2007.

[32] A. H. Tadao Sugiura, Saki Maeda, "Pulse laser assisted optical tweezers for biomedical applications," *Annual International Conference of the IEEE Engineering in Medicine and Biology Society. IEEE Engineering in Medicine and Biology Society. Annual International Conference*, vol. 2012, pp. 4479–4481, 2012.

[33] I. Heller, T. P. Hoekstra, G. A. King, E. J. G. Peterman, and G. J. L. Wuite, "Optical tweezers analysis of dna–protein complexes," *Chemical Reviews*, vol. 114, no. 6, pp. 3087–3119, 2014.

[34] M. D. Wang, H. Yin, R. Landick, J. Gelles, and S. M. Block, "Stretching dna with optical tweezers," *Biophysical journal*, vol. 72, no. 3, pp. 1335–1346, 1997.

[35] A. Keloth, O. Anderson, D. Risbridger, and L. Paterson, "Single cell isolation using optical tweezers," *Micromachines*, vol. 9, no. 9, p. 434, 2018.

[36] A. Atajanov, A. Zhbanov, and S. Yang, "Sorting and manipulation of biological cells and the prospects for using optical forces," *Micro and Nano Systems Letters*, vol. 6, dec 2018.

[37] C. Arbore, L. Perego, M. Sergides, and M. Capitanio, "Probing force in living cells with optical tweezers: from single-molecule mechanics to cell mechanotransduction," *Biophysical reviews*, 10 2019.

[38] D. J. Armstrong, T. A. Nieminen, A. B. Stilgoe, A. V. Kashchuk, I. C. D. Lenton, and H. Rubinsztein-Dunlop, "Swimming force and behavior of optically trapped microorganisms," *Optica*, vol. 7, no. 8, pp. 989–994, Aug 2020.

[39] I. A. Carvalho, N. A. Silva, C. C. Rosa, L. C. C. Coelho, and P. A. S. Jorge, "Particle classification through the analysis of the forward scattered signal in optical tweezers," *Sensors*, vol. 21, no. 18, p. 6181, 2021.

[40] P. A. Jorge, I. A. Carvalho, F. M. Marques, V. Pinto, P. H. Santos, S. M. Rodrigues, S. P. Faria, J. S. Paiva, and N. A. Silva, "Classification of optically trapped particles: A comparison between optical fiber tweezers and conventional setups," *Results in Optics*, vol. 5, p. 100178, 2021.

[41] N. Cennamo, G. D'Agostino, G. Porto, A. Biasiolo, C. Perri, F. Arcadio, and L. Zeni, "A molecularly imprinted polymer on a plasmonic plastic optical fiber to detect perfluorinated compounds in water," *Sensors*, vol. 18, no. 6, 2018.

[42] N. Cennamo, G. D'Agostino, C. Perri, F. Arcadio, G. Chiaretti, E. M. Parisio, G. Camarlinghi, C. Vettori, F. Di Marzo, R. Cennamo, G. Porto, and L. Zeni, "Proof of concept for a quick and highly sensitive on-site detection of sars-cov-2 by plasmonic optical fibers and molecularly imprinted polymers," *Sensors*, vol. 21, no. 5, 2021.

[43] R. Lorenzo, A. Carro, C. Alvarez-Lorenzo, and A. Concheiro, "To remove or not to remove? the challenge of extracting the template to make the cavities available in molecularly imprinted polymers (mips)," *International journal of molecular sciences*, vol. 12, pp. 4327–47, 12 2011.

[44] G. Pesce, P. Jones, O. Maragò, and G. Volpe, "Optical tweezers: theory and practice," *The European Physical Journal Plus*, vol. 135, 12 2020.

[45] P. H. Jones, O. M. Maragò, and G. Volpe, *Optical Tweezers: Principles and Applications*. Cambridge University Press, 2015.

[46] K. C. Neuman and S. M. Block, "Optical trapping." *The Review of scientific instruments*, 2004.

[47] F. L. Pedrotti, L. M. Pedrotti, and L. S. Pedrotti, *Introduction to Optics*, 3rd ed. Cambridge University Press, 2017.

[48] A. Callegari, M. Mijalkov, A. B. Gököz, and G. Volpe, "Computational toolbox for optical tweezers in geometrical optics," *J. Opt. Soc. Am. B*, vol. 32, no. 5, pp. B11–B19, May 2015.

[49] A. R. da Silva Rodrigues Ribeiro, "Optical fiber tools for single cell trapping and manipulation," Ph.D. dissertation, 2017. [Online]. Available: https://hdl.handle.net/10216/109237

[50] A. Ashkin, "Forces of a single-beam gradient laser trap on a dielectric sphere in the ray optics regime," *Biophysical Journal*, vol. 61, no. 2, pp. 569–582, 1992.

[51] K. Berg-Sørensen and H. Flyvbjerg, "Power spectrum analysis for optical tweezers," *Review of Scientific Instruments*, vol. 75, no. 3, pp. 594–612, 2004.

[52] P. Wu, R. Huang, C. Tischer, and E.-L. Florin, "Measurement of the non-conservative force generated by optical tweezers," *Biophysical Journal*, vol. 96, no. 3, p. 289a, feb 2009.

[53] R. Goerlich, M. Li, S. Albert, G. Manfredi, P.-A. Hervieux, and C. Genet, "Noise and ergodic properties of brownian motion in an optical tweezer: Looking at regime crossovers in an ornstein-uhlenbeck process," *Phys. Rev. E*, vol. 103, p. 032132, Mar 2021.

[54] I. A. Carvalho, "Analytical tweezers for cell manipulation and diagnostic," Master's thesis, Faculty of Science of University of Porto, 2021.

[55] A. Bui, A. Kashchuk, M. Balanant, T. Nieminen, H. Rubinsztein-Dunlop, and A. Stilgoe, "Calibration of force detection for arbitrarily shaped particles in optical tweezers," *Scientific Reports*, vol. 8, 07 2018.

[56] S. Nørrelykke, E. Schäffer, J. Howard, F. Pavone, F. Jülicher, and H. Flyvbjerg, "Calibration of optical tweezers with positional detection in the back-focal-plane," *Review of Scientific Instruments*, vol. 77, 04 2006.

[57] M. A. de Araújo, R. Silva, E. de Lima, D. P. Pereira, and P. C. de Oliveira, "Measurement of gaussian laser beam radius using the knife-edge technique: improvement on data analysis," *Appl. Opt.*, vol. 48, no. 2, pp. 393–396, Jan 2009.

[58] V. Dudelev, "Optical trapping with superfocused high-m2 laser diode beam," *Proceedings of SPIE - The International Society for Optical Engineering*, vol. 9343, p. 93430Q, 03 2015.

[59] M. Grabe, "Measurement uncertainties in science and technology," *Measurement Uncertainties in Science and Technology: , ISBN 978-3-540-20944-7. Springer-Verlag Berlin Heidelberg, 2005*, 01 2005.

[60] M. F. Mohamad Yusof, M. Yeng, and S. K. Ayop, "Axial calibration of qpd signal based on stuck bead method for optical trapping applications," *International Journal of Engineering & Technology*, vol. 7, p. 371, 11 2018.

[61] F. Coutinho, J. Teixeira, V. Rocha, J. Oliveira, P. A. S. Jorge, and N. A. Silva, "Autonomous optical tweezers: from automatic trapping to single particle analysis," 2022.

[62] J. Teixeira, V. Rocha, J. Oliveira, P. A. S. Jorge, and N. A. Silva, "Towards real-time identification of trapped particles with umap-based classifiers," 2022.

[63] V. Rocha, J. Oliveira, A. Guerreiro, P. A. S. Jorge, and N. A. Silva, "Intelligent optical tweezers with deep neural network classifiers," 2022.

[64] J. Zempleni, S. S. Wijeratne, and Y. I. Hassan, "Biotin," *Biofactors*, vol. 35, no. 1, pp. 36–46, 2009.

[65] J. Herranen, J. Markkanen, G. Videen, and K. Muinonen, "Non-spherical particles in optical tweezers: A numerical solution - Fig 18," 12 2019.

[66] I. Lenton, D. Armstrong, A. Stilgoe, T. Nieminen, and H. Rubinsztein-Dunlop, "Orientation of swimming cells with annular beam optical tweezers," vol. 459, 11 2019.